6-21-2017 12:00 AM

Efficient Macromodeling and Fast Transient Simulation of High Speed Distributed Interconnects

Sadia Wahid, *The University of Western Ontario*

Supervisor: Dr. Anestis Dounavis, *The University of Western Ontario*

A thesis submitted in partial fulfillment of the requirements for the Master of Engineering Science degree in Electrical and Computer Engineering

Abstract

In the first part of the thesis, an efficient macromodeling technique based on Loewner Matrix (LM) approach has been presented to model multi-port distributed systems using tabulated noisy data. In the proposed method, Loewner Model data from previous rational approximation are used to create less noisy eigenvectors in an iterative manner. As a result, the biasing effect of the LM model approximated by the noisy data is reduced. It is illustrated that this method improves the accuracy of the Loewner Matrix modeling for noisy frequency data.

In the second part, a fast and robust algorithm is introduced for time-domain simulation of interconnects with few nonlinear elements based on Large Change Sensitivity approach. After macromodeling interconnects, linear parts of the system construct very large matrix. Large linear matrix with nonlinear components makes time domain simulation a Central Processing Unit (CPU) intensive task where inversion (one Lower/Upper (LU) decomposition and one forward/backward substitution) of this large matrix is done at each step of the Newton-Raphson iteration. Using the proposed method, large system matrix is partitioned into linear and nonlinear parts and LU decomposition of linear matrix is done only once in the entire simulation. Nonlinear elements construct a very small matrix compared to large linear matrix. In this proposed method, small matrix is inverted at each Newton iteration. Cost of inverting a small matrix is much cheaper than inverting a very large matrix. Therefore, this approach is faster than the conventional matrix inversion method. Numerical examples are presented illustrating validity and efficiency of the above method.

Keywords: Frequency domain modeling, interconnect modeling, iterative Loewner method, large change sensitivity, noisy frequency responses, transient analysis.

Acknowledgment

I would like to express my gratitude to my supervisor Dr. Anestis Dounavis for his guidance, continuous encouragement, friendly motivation, patience, and his valuable advice during my research journey. I am grateful to him for introducing me to the area of interconnect modeling and simulations. Without his guidance and help this dissertation would not have been possible.

Moreover, I am thankful towards my colleagues: Tarik Menkad and Mohamed Sahouli for sharing their knowledge and study materials, Sharath Manjunath for his help to set up my lab desk and computer and Sara Mantach for her friendly conversations during my study period.

I would like to thank my family and friends for their motivation and persuasion throughout my Master's work. Finally, I must give greatest appreciation to my parents, for their love, inspiration and support during my life so far.

Dedication

To

my

Grandparents

Contents

List of Figures

List of Tables

List of Abbreviations

VLSI Very Large Scale Integration.

LM Loewner Matrix.

MNA Modified Nodal Analysis.

DS Descriptor System.

LU Lower-Upper matrix decomposition.

ODE Ordinary Differential Equations.

LCS Large Change Sensitivity.

PDE Partial Differential Equations.

SNR Signal-to-Noise Ratio.

VF Vector Fitting.

MoC Method of Characteristics.

PRIMA Passive Reduced-order Interconnect Macromodeling Algorithm.

SVD Singular Value Decomposition.

VNA Vector Network Analyzer.

Chapter 1

Introduction

1.1 Background and Motivation

Advances in Very-Large-Scale-Integration (VLSI) technology have made phenomenal growth in operating speed, densities and diminishing device sizes. With increasing frequency, interconnect analysis has become a major requirement for all state-of-the-art circuit design and simulations. Interconnects can exist at various levels such as on-chip, packaging structures, vias, printed circuit boards (PCB) and backplanes etc. Once neglected interconnect effects such as ringing, signal delay, distortion and attenuation give rise to signal integrity issues [1–5]. Accurate capture of signal integrity issues at early stage of design ensures circuit performance and reliability [1].

Circuit simulators like SPICE face difficulties to simulate interconnects in the presence of nonlinear components due to mixed frequency/time problem as well as CPU inefficiency. This is because, characteristics of interconnects are governed by Telegrapher's equations which are Partial Differential Equations (PDEs) and are best solved in the frequency domain, whereas nonlinear elements are described only in the time domain with nonlinear Ordinary Differential Equations (ODEs). Different numerical macromodeling techniques are used to convert PDEs to ODEs to simulate interconnects with nonlinear elements [1, 3, 5, 6].

At first we can divide interconnect macromodeling strategies into two cases. In the first case, physical characteristics of the interconnect structure are known and modeling is based on Quasi-Transverse Electromagnetic mode of propagation of waves. In the second case, where physical structure is unknown or any analytic solution is hard to derive, rational macromodeling approximation from full-wave electromagnetic simulation or port-port measured data are used to model interconnects [7].

Two types of macromodeling are done with known physical characteristics of interconnects. One is rational approximation and other is delay extraction based modeling techniques. Brute force lumped segmentation modeling [8], passive reduced-order interconnect macromodeling algorithm (PRIMA) [9], matrix rational approximation (MRA) [10, 11], compact difference [12], integral congruent transformation [13, 14] are included under rational approximation modeling. These modeling algorithms are passive by construction. However, they require high order approximation to capture the delay. On the other hand, delay extraction method like Method of Characteristics (MoC) [15] use a low order approximation as the delay of the transfer function is extracted. However, MoC is not passive by construction.

Macromodeling algorithms for interconnects with no prior knowledge of the physical characteristics are based on frequency domain, multiport tabulated data obtained either from electromagnetic simulations or from measurements [16–37]. Frequency domain data are often presented in the form of impedance, hybrid, scattering or admittance parameters data. One approach to convert frequency domain data into time domain analysis is based on convolution techniques [19, 20]. However, this approach is time consuming [21] and requires high memory allocation [22]. Another approach is to generate closed form time domain macromodels. These methods approximate the transfer function in descriptor system (DS) or pole-residue format. They can be directly incorporated into modified nodal analysis equations [23] or recursive convolution can be used to obtain transient response [24].

A popular pole-residue based system identification tool is called Vector Fitting (VF) [16] which is formulated as a linear least squares problem and depends on an iterative pole relocation

approach to improve the approximation. Various enhancements have been made to improve its accuracy and efficiency [25–27]. VF has also been used for multiport network using QR decomposition and parallel processing [28]. In recent years, Loewner Matrix (LM) [29–31] framework has been proposed to generate descriptor state-space models from frequency domain measured data of interconnect network. Unlike VF, LM method is very efficient to identify the system from the tabulated data with fewer state-space equations [29, 31]. In Loewner Matrix modeling, order of the system can be identified from the Singular Value Decomposition (SVD) of Loewner Matrix [29]. Delay extraction based Loewner modeling method has been proposed in [32] to approximate a low-order rational model.

In the presence of noise in frequency domain data, several modifications have been proposed for vector fitting algorithm. They are such as pole adding and skimming method [33], least squares weighted functions [34] and instrumental variable VF method [35]. Moreover, LM interpolation method faces some issues to accurately identify the system from contaminated frequency domain data [36]. In [36] which pole/residues are relevant based on examining the norms of the residues and in [37] an iterative least square based LM interpolation approximation are proposed to identify system from noisy data, respectively.

After macromodeling interconnects, nonlinear components like drivers and receivers are included in time domain circuit simulations. For transient analysis, integration techniques are used to convert differential equations into difference equations. To solve the difference equations with nonlinear elements at each time step, Newton-Raphson iterations are required. Modeling of interconnects leads to large circuit matrix making time-domain analysis a CPU intensive task for nonlinear circuit simulators [3]. In order to address the above issue, a fast and efficient algorithm for transient analysis of large interconnect network is presented in this thesis.

1.2 Objectives

The first objective of this thesis is to develop an algorithm to improve the accuracy of the identified state-space system from the noisy data based on Loewner modeling approach. The second objective is to apply Large Change Sensitivity (LCS) [38,39] approach for fast transient analysis of interconnects circuits including nonlinear loads, drivers and receivers.

1.3 Contributions

The main contributions of the thesis are as follows:

1. An iterative algorithm is proposed to create less noisy data from previous Loewner Matrix approximated model. Then this data is used to create less noisy eigenvectors. As a result, the biasing effect of the LM solution caused by the noise of the eigenvectors created from original data is reduced by this method.

2. This proposed iterative method has been applied to multiport network. Numerical examples are presented to compare the LM based approximation and proposed iterative LM approximated models.

3. Large Change Sensitivity approach is used for fast transient analysis of large distributed networks terminated with nonlinear loads and drivers.

4. LM method has been used to model large interconnect network from measured frequency data. Loewner method together with Large Change Sensitivity (LCS) approach is used for transient analysis of nonlinear distributed networks.

1.4 Organization of the Thesis

The organization of the thesis is as follows. Chapter 2 gives brief review of interconnects modeling, modified nodal analysis of linear and nonlinear distributed networks and transient analysis of nonlinear networks. Chapter 3 develops an efficient method to macromodel large

multiport systems characterized by noisy frequency domain data, using an iterative Loewner Matrix algorithm. It is illustrated that the proposed approach can increase the accuracy of the Loewner modeling with noisy tabulated data. Chapter 4 discusses a fast transient analysis algorithm based on Large Change Sensitivity approach. Here distributed interconnect network has been modeled using lumped modeling and Loewner matrix modeling techniques. Time and accuracy have been compared between conventional matrix inversion and proposed approach for transient analysis for both modeling approaches. Finally, Chapter 5 summarises the work proposed along with some future research suggestions.

Chapter 2

High Speed Interconnects

2.1 Introduction

Interconnects propagate signals between electrical devices. At low frequencies, they behave like short circuits. As the frequency increases, they start to behave like transmission lines and are responsible for signal degradation in the circuit. Modern VLSI circuits have made modeling and analyzing of interconnects a necessary task. The aim of this chapter is to review some of the interconnect macromodels and numerical techniques that are used for interconnect analysis.

2.2 Interconnect Modeling

Interconnect modeling depends on the physical structure as well as the operating frequency of the electrical circuit. *Electrical length* of interconnects is an essential factor to model and analyze them. Interconnects are considered to be *'electrically short'*, if they are physically shorter than one-tenth of the wavelength of the operating signal [3].

$$\frac{l}{\lambda} < 0.1; \quad \lambda = \frac{v}{f} \tag{2.1}$$

where l is the interconnect length, λ is the signal wavelength, v is the propagation velocity and f is the frequency. Otherwise, interconnects are considered,*'electrically long'*. A practical relationship between maximum frequency denoted by f_{max} and rise time represented as t_r of a signal can be expressed as [3, 40],

$$f_{max} \approx \frac{0.35}{t_r} \tag{2.2}$$

Figure 2.1 shows the top view and cross sectional view of an interconnect system consists of

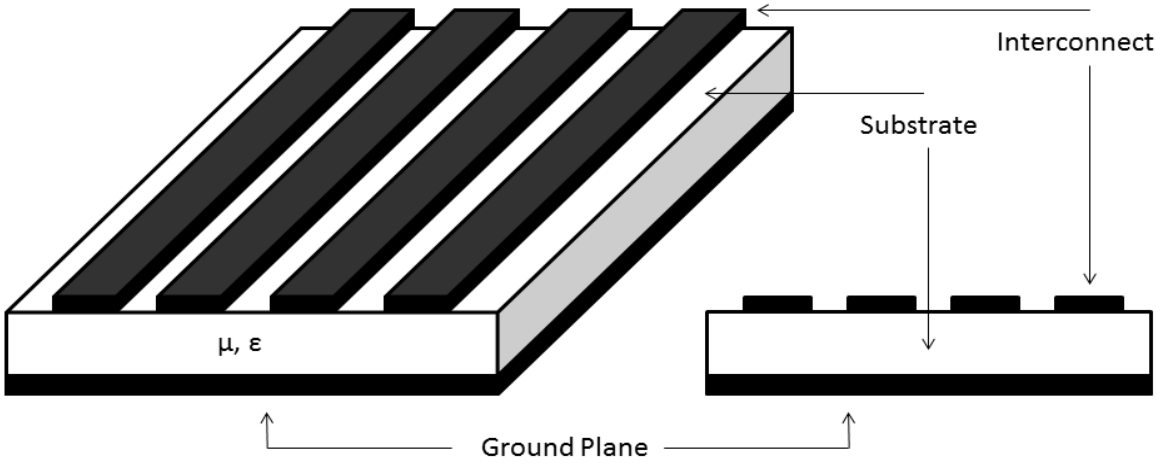

Figure 2.1: Interconnect system top view and cross sectional view

four conductors and ground plane. Modeling of interconnects depends on the operating frequency, signal rise and fall times, length of interconnects and their physical properties. These factors determine whether the modeling of interconnects is based on quasi-transverse electromagnetic (quasi-TEM) or full wave assumptions. For interconnect structure that cannot be modeled analytically, linear networks characterized by tabulated or measured data have been proposed.

2.3 Quasi-Transverse Electromagnetic Models

Transverse electromagnetic (TEM) waves exist for interconnects with homogeneous mediums and perfect conductors [2]. Under these conditions, interconnects produce electric and magnetic fields that are transverse or perpendicular to one another and to the direction of propagation. Quasi-TEM assumptions remain the dominant trend for analyzing interconnects, since the approximation is valid for most practical structures and offers relative ease and low computation cost compared to full wave approaches [3, 5].

The voltages and currents for interconnects under quasi-TEM assumption are described by partial differential equations (PDEs) known as Telegrapher's equations,

$$\begin{aligned} \frac{\partial v(x,t)}{\partial x} &= -Ri(x,t) - L\frac{\partial i(x,t)}{\partial t} \\ \frac{\partial i(x,t)}{\partial x} &= -Gv(x,t) - C\frac{\partial v(x,t)}{\partial t} \end{aligned} \tag{2.3}$$

where voltage $v(x,t)$ and current $i(x,t)$ are functions of position x and time t; R, L, C and G are the per unit length (p.u.l.) resistance, inductance, capacitance and conductance of the interconnect respectively. The p.u.l parameters are obtained from the cross-sectional dimensions and physical characteristics of the transmission line. They are also used to determine voltages and currents of the transmission line [2].

2.3.1 Distributed Lumped Modeling

Lumped segmentation technique uses lumped resistive-inductive-conductive-capacitive (RLGC) model of the transmission lines to approximate Telegrapher's equations. Applying Euler's method [2] to (2.3) yields

$$\begin{aligned} v(x+\Delta x,t) - v(x,t) &= -\Delta x Ri(x,t) - \Delta x L\frac{\partial i(x,t)}{\partial t} \\ i(x+\Delta x,t) - i(x,t) &= -\Delta x Gv(x+\Delta x,t) - \Delta x C\frac{\partial v(x+\Delta x,t)}{\partial t} \end{aligned} \tag{2.4}$$

where $x = [1, 2, ..., \eta]$, $\Delta x = l/\eta$, η is the number of sections and l is the length of interconnect. Equation (2.4) can be implemented by lumped equivalent circuit composed of resistors, inductors, conductors, and capacitors.

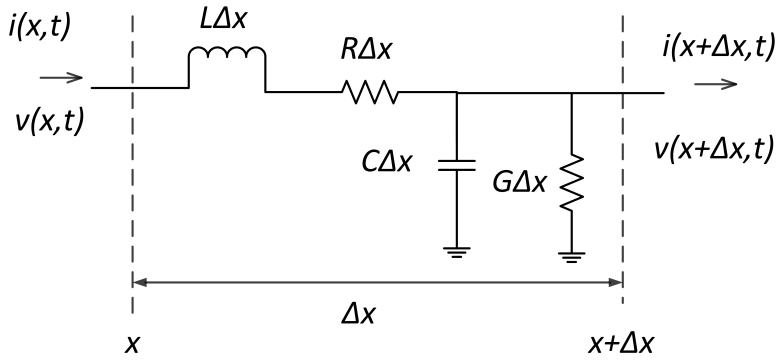

Figure 2.2: Distributed Lumped model segment

Figure 2.2 shows the general lumped component for a two conductor transmission line. HSPICE [41] use equation (2.5) in order to estimate the number of sections for time domain analysis of interconnects.

$$\eta = 20\frac{l.\sqrt{LC}}{t_r} \tag{2.5}$$

where t_r is the rise/fall time. The lumped segmentation model is passive and provides a direct method to discretize interconnects. However the approximation is only valid if Δx is chosen to be a small fraction of the wave length. If the rise/fall time is fast or if the interconnect is electrically long, many lumped segments are required for an accurate model. This leads to large circuit matrix increasing CPU time for time domain simulation.

2.3.2 Method of Characteristics

Another most commonly used algorithms to model interconnect are based on the generalized method of characteristics (MoC) [15, 22, 42–46]. In MoC, the line propagation delay is ex-

tracted and exact models are produced applying to lossless transmission lines [15]. These methods are also applied to model lossy MTLs [42–46]. The MoC is based on extracting the propagation delay allowing the attenuation function to be approximated with a low order rational transfer function. It reduces the computation complexity for long lines with low losses. The original method of characteristics [15] or Branin's method was used to represent interconnects as ODEs containing time delays. Although it was developed in the time-domain using characteristics curves (hence the name), a simpler alternative in the frequency domain is presented here. The frequency domain solution of Telegrapher's equation for two-conductor transmission lines (one signal conductor and another reference conductor) [46] is

$$\begin{bmatrix} I_1 \\ I_2 \end{bmatrix} = \frac{1}{Z_0(1-e^{-2\gamma l})} \begin{bmatrix} 1+e^{-2\gamma l} & -2e^{-\gamma l} \\ -2e^{-\gamma l} & 1+e^{-2\gamma l} \end{bmatrix} \begin{bmatrix} V_1 \\ V_2 \end{bmatrix} \tag{2.6}$$

$$\gamma = \sqrt{(R+sL)(G+sC)} \qquad Z_0 = \sqrt{\frac{R+sL}{G+sC}}$$

where γ is the propagation constant and Z_0 is the characteristics impedance.

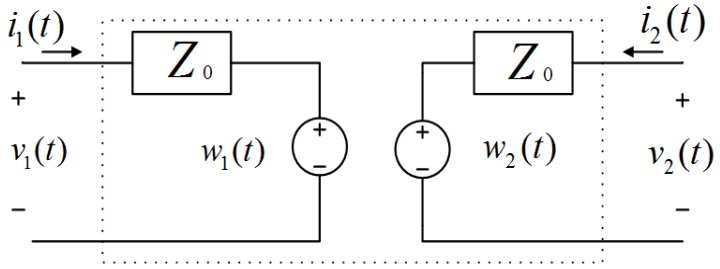

Figure 2.3: Transmission Line Model for Method of Characteristics

After some re-arrangement, the terms in (2.6) can be expressed as,

$$V_1 = Z_0 I_1 + W_1$$

$$V_2 = Z_0 I_2 + W_2 \tag{2.7}$$

Here W_1 and W_2 have a recursive relation as

$$\begin{aligned} W_1 &= e^{-\gamma l}(2V_2 - W_2) \\ W_2 &= e^{-\gamma l}(2V_1 - W_1) \end{aligned} \tag{2.8}$$

For lossless transmission lines, $R = 0$ and $G = 0$. Thus γ and Z_0 reduces to

$$\gamma = s\sqrt{LC} \qquad Z_0 = \sqrt{\frac{L}{C}} \tag{2.9}$$

As a result, γ becomes purely imaginary and Z_0 becomes a real constant. By taking the inverse Laplace transform of (2.7) & (2.8), we can get the time domain solution of MoC as,

$$\begin{aligned} v_1(t) &= Z_0 i_1(t) + w_1(t) \\ v_2(t) &= Z_0 i_2(t) + w_2(t) \\ w_1(t+\tau) &= 2v_2(t) - w_2(t) \\ w_2(t+\tau) &= 2v_1(t) - w_1(t) \end{aligned} \tag{2.10}$$

where $\tau = \gamma l$ is a delay term in the time-domain. A transmission line model for MoC in time-domain is shown in Figure 2.3. For lossy transmission lines, γ is not purely imaginary and Z_0 is not a real constant. They are irrational function of complex frequency s. As a result, direct time domain representation is not possible. In this case, rational approximation of γ and Z_0 has been proposed [42–46] for lossy transmission line models.

Therefore, γ and Z_0 are approximated as,

$$Z_0 = Z_0(s) \simeq \sum_n \frac{R_n^Z}{s - p_n^Z} + Z_\infty$$

$$\gamma = \gamma(s) = \sqrt{(R + sL)(G + sC)} \approx s\sqrt{L_\infty C_\infty} + P(s)$$

$$P(s) \simeq \sum_n \frac{R_n^P}{s - p_n^P} + P_\infty$$

Here $Z_0(s)$ and $P(s)$ are approximated in pole residue form. R_n^Z and p_n^Z are real or complex residues and poles of $Z_0(s)$. R_n^P and p_n^P are real or complex residues and poles of $P(s)$. L_∞, C_∞ are inductance and capacitance at $s = j\infty$ respectively.

2.4 Full Wave Models

If the cross-sectional dimensions of interconnects become a significant fraction of the circuits operating wavelength, field components in the direction of propagation can no longer be ignored [47]. Under these conditions, quasi-TEM assumptions become inadequate to describe interconnect and full wave models are required.

Full wave models provide better accuracy when compared to quasi-TEM models. However, full wave models are not used by circuit simulators because of the expensive CPU requirements [48]. The cost of full wave simulation associated with each interconnect at a particular frequency point is extremely high. Generally, high speed interconnects require thousands of frequency points to accurately model the response of the system. The cost of the computation of the full wave model combined with the evaluation cost of the overall circuit makes the technique unreasonably expensive to use in circuit simulation.

Another problem with full wave methods is to represent the model in the circuit simulator. The information provided by wave full wave analysis is in terms of field parameters such as propagation constants, characteristic impedances, current eigenvectors, etc. Circuit simulators require information in terms of voltages, currents and impedances. Therefore, an interface

needs to be developed to link full wave methods into circuit simulators.

2.5 Measured Data Model

For interconnects having geometric inhomogeneity and discontinuities, sometimes it is not possible to obtain accurate analytical physics based models. To overcome this issue, modeling techniques based on measured data or tabulated data have been proposed [49,50]. Interconnects are modeled using measured data from frequency dependent scattering parameters, electromagnetic simulations or by time domain terminal measurements. Time domain measurements can be acquired by numerical solution of the electromagnetic field problems [51, 52] or by time domain reflectometry (TDR) methods [53]. Measured data obtained by different methods are contaminated by noise. To decrease the impact of noise, large data sets are required.

2.5.1 Vector Fitting

Vector fitting (VF) uses an iterative approach to acquire a rational function to approximate the data obtained by measurement or electromagnetic simulation. It was first introduced by Gustavsen in 1998 and many developments have been made over the years in [16, 54–57].

The objective of vector fitting is to determine a rational approximation of a set of measured data $\{s, \boldsymbol{Y}(s)\}$ as,

$$f(s) = \sum_{n=1}^{N} \frac{r_n}{s - p_n} + d + se \tag{2.11}$$

where r_n and p_n correspond to real or conjugate residues and poles respectively, while the real variables d and e are optional; s is the Laplace variable, $\boldsymbol{Y}(s)$ is the measured data value at s and N is the number of poles and residues or the order of the rational function. The nonlinear problem in (2.11) can be solved by following two steps. The first step is an iterative pole identification process and the second step is to identify the residues using a least square approximation. To obtain an approximation for the poles p_n, an unknown function $\alpha(s)$ is

introduced as,

$$\alpha(s) = \sum_{n=1}^{N} \frac{\tilde{r}_n}{s - \tilde{p}_n} + 1 \tag{2.12}$$

where $\tilde{p}_n$ are the starting poles and the remaining terms are unknowns. In addition, the rational approximation for $\alpha(s)f(s)$ can be described as,

$$\alpha(s)f(s) \cong (\alpha f)(s) = \sum_{n=1}^{N} \frac{r_n}{s - \tilde{p}_n} + d + se \tag{2.13}$$

Multiplying (2.12) by $f(s)$ and equating with (2.13), yields the following system of equation,

$$\sum_{n=1}^{N} \frac{r_n}{s - \tilde{p}_n} + d + se = (\sum_{n=1}^{N} \frac{\tilde{r}_n}{s - \tilde{p}_n} + 1)f(s) \tag{2.14}$$

This linear problem has r_n, $\tilde{r}_n$, d and e as unknowns. For each frequency point s_j, the system of (2.14) can be expressed as,

$$A_j X = b_j \tag{2.15}$$

where

$$\begin{aligned} A_j &= \begin{bmatrix} Re(z_1^j) & .... & Re(z_N^j) & 1 & 0 & Re(\tilde{z}_1^j) & .... & Re(\tilde{z}_N^j) \\ Im(z_1^j) & .... & Im(z_N^j) & 1 & 0 & Im(\tilde{z}_1^j) & .... & Im(\tilde{z}_N^j) \end{bmatrix} \\ X &= \begin{bmatrix} r_1 & .... & r_N & d & e & \tilde{r}_1 & .... & \tilde{r}_N \end{bmatrix} \\ b_j &= \begin{bmatrix} Re(Y(s_j)) \\ Im(Y(s_j)) \end{bmatrix} \end{aligned} \tag{2.16}$$

For real poles and residues, the coefficients of (2.16) will become,

$$z_k^j = \frac{1}{s_j - \tilde{p}_k}; \qquad \tilde{z}_k^j = \frac{-Y(s_j)}{s_j - \tilde{p}_k}$$

For complex conjugate pole and residue pairs, the coefficients of (2.16) will be

$$z_k^j = \frac{1}{s_j - \tilde{p}_k} + \frac{1}{s_j - \tilde{p}_{k+1}}; \quad z_{k+1}^j = \frac{i}{s_j - \tilde{p}_k} - \frac{i}{s_j - \tilde{p}_{k+1}}$$
$$\tilde{z}_k^j = \frac{-Y(s_j)}{s_j - \tilde{p}_k} + \frac{-Y(s_j)}{s_j - \tilde{p}_{k+1}}; \quad \tilde{z}_{k+1}^j = \frac{-iY(s_j)}{s_j - \tilde{p}_k} + \frac{iY(s_j)}{s_j - \tilde{p}_{k+1}}$$
$$r_k = Re(r_k); \quad r_{k+1} = Re(r_k)$$
$$\tilde{r}_k = Re(\tilde{r}_k); \quad \tilde{r}_{k+1} = Re(\tilde{r}_k)$$

From all the above equations, an overdetermined system of equation can be formed for all the frequency points as,

$$AX = b \tag{2.17}$$

The solution of X can be obtained by the least square solution by doing,

$$X = (A^T A)^{-1}(A^T b) \tag{2.18}$$

From the least square solution of (2.18), we can get approximations for $\alpha(s)$ and $(\alpha f)(s)$ and they can be written as,

$$\alpha(s)_{fit} = \frac{\prod_{n=1}^{N}(s - \tilde{a}_n)}{\prod_{n=1}^{N}(s - \tilde{p}_n)}$$
$$(\alpha f)_{fit}(s) = e\frac{\prod_{n=1}^{N+1}(s - a_n)}{\prod_{n=1}^{N}(s - \tilde{p}_n)} \tag{2.19}$$

The poles of (2.19) cancel each other out to get a rational approximation for $f(s)$ as,

$$f(s) = \frac{(\alpha f)_{fit}(s)}{\alpha(s)_{fit}} = e\frac{\prod_{n=1}^{N+1}(s - a_n)}{\prod_{n=1}^{N}(s - \tilde{a}_n)} \tag{2.20}$$

where the zeros of $\alpha(s)_{fit}$ becomes the poles of $f(s)$. By taking this new set of poles $\tilde{a}_n$ as the new guess for the next iterations to replace previous poles p_n. This iterative procedure is continued until convergence.

After the poles of the system are determined, an additional least square solution is needed for the residues to obtain and the terms d and e if they are present in the system.

2.5.2 Loewner Matrix Model

In time domain, a multiport Linear Time Invariant (LTI) system with P inputs and outputs can be described as a state-space model:

$$\begin{aligned} \boldsymbol{E}\dot{x}(t) &= \boldsymbol{A}x(t) + \boldsymbol{B}u(t) \\ y(t) &= \boldsymbol{C}x(t) + \boldsymbol{D}u(t) \end{aligned} \tag{2.21}$$

where $x(t) \in \mathbb{R}^r$ vector contains internal variables, $u(t) \in \mathbb{R}^P$ and $y(t) \in \mathbb{R}^P$ vectors contains input and output port voltages and currents, respectively. The matrices $\boldsymbol{E}, \boldsymbol{A} \in \mathbb{R}^{r\times r}$, $\boldsymbol{B} \in \mathbb{R}^{r\times P}$, $\boldsymbol{C} \in \mathbb{R}^{P\times r}$, $\boldsymbol{D} \in \mathbb{R}^{r\times P}$ describe the system and r is the order of the system. The closed form expression of frequency domain Y-parameters of the LTI system in (2.21) can be presented by,

$$\boldsymbol{Y}(s) = \boldsymbol{C}(s\boldsymbol{E} - \boldsymbol{A})^{-1}\boldsymbol{B} + \boldsymbol{D} \tag{2.22}$$

Loewner Matrix method [29–31] is used to get a time domain macromodel from the frequency domain measured or simulated data. Frequency domain data are often presented in the form of impedance, hybrid, scattering (S-parameter) or admittance (Y-parameter) parameter data.

The frequency domain data is expressed as,

$$\{s_m, \boldsymbol{Y}(s_m)\} \tag{2.23}$$

where s_m is the complex frequency, $\boldsymbol{Y}(s_m)$ is the S-parameter or Y-parameter data at frequency s_m and $m = 1, 2, \ldots, M$, where M is the number of data points. The frequency data is splitted

into odd and even data points as follows:

$$\begin{aligned}\{s_1,\ldots,s_M\} &= \{\tau_1,\ldots,\tau_{\overline{m}}\}\cup\{\upsilon_1,\ldots,\upsilon_{\underline{m}}\}\\ \{\boldsymbol{Y}(s_1),\ldots,\boldsymbol{Y}(s_M)\} &= \{\boldsymbol{Y}(\tau_1),\ldots,\boldsymbol{Y}(\tau_{\overline{m}})\}\cup\{\boldsymbol{Y}(\upsilon_1),\ldots,\boldsymbol{Y}(\upsilon_{\underline{m}})\}\\ \{\boldsymbol{Y}(\tau_1),\ldots,\boldsymbol{Y}(\tau_{\overline{m}})\} &= \{W_1,\ldots,W_{\overline{m}}\}\\ \{\boldsymbol{Y}(\upsilon_1),\ldots,\boldsymbol{Y}(\upsilon_{\underline{m}})\} &= \{U_1,\ldots,U_{\underline{m}}\}\end{aligned} \tag{2.24}$$

Here $\overline{m}+\underline{m}=M$.

$$\overline{m}=\underline{m}=\frac{M}{2}\qquad\text{Here M is even}$$
$$\overline{m}=\underline{m}+1=\frac{M+1}{2}\qquad\text{Here M is odd}$$

Here frequency data is splitted into odd and even data points.

Right data set:

$\boldsymbol{\Gamma}$= diag$[\tau_1,\ldots,\tau_{\overline{m}}]\in\mathbb{C}^{\overline{m}\times\overline{m}}$, $\boldsymbol{R}=[R_1,\ldots,R_{\overline{m}}]\in\mathbb{C}^{P\times\overline{m}}$, $\boldsymbol{W}=[W_1,\ldots,W_{\overline{m}}]\in\mathbb{C}^{P\times\overline{m}}$

Left data set:

$\boldsymbol{\Upsilon}$= diag$[\upsilon_1,\ldots,\upsilon_{\underline{m}}]\in\mathbb{C}^{\underline{m}\times\underline{m}}$, $\boldsymbol{L^T}=[L_1,\ldots,L_{\underline{m}}]\in\mathbb{C}^{\underline{m}\times P}$, $\boldsymbol{U^T}=[U_1,\ldots,U_{\underline{m}}]\in\mathbb{C}^{\underline{m}\times P}$

Here $\boldsymbol{R}$ and $\boldsymbol{L}$ are random matrices. Loewner matrix $\mathbb{L}$ and shifted Loewner Matrix $\sigma\mathbb{L}$ are calculated as:

$$\mathbb{L}=\begin{bmatrix}\frac{U_1R_1-L_1W_1}{\upsilon_1-\tau_1} & \cdots & \frac{U_1R_{\overline{m}}-L_1W_{\overline{m}}}{\upsilon_1-\tau_{\overline{m}}}\\ \vdots & \ddots & \vdots\\ \frac{U_{\underline{m}}R_1-L_{\underline{m}}W_1}{\upsilon_{\underline{m}}-\tau_1} & \cdots & \frac{U_{\underline{m}}R_{\overline{m}}-L_{\underline{m}}W_{\overline{m}}}{\upsilon_{\underline{m}}-\tau_{\overline{m}}}\end{bmatrix} \tag{2.25}$$

$$\sigma\mathbb{L}=\begin{bmatrix}\frac{\upsilon_1U_1R_1-\tau_1L_1W_1}{\upsilon_1-\tau_1} & \cdots & \frac{\upsilon_1U_1R_{\overline{m}}-\tau_{\overline{m}}L_1W_{\overline{m}}}{\upsilon_1-\tau_{\overline{m}}}\\ \vdots & \ddots & \vdots\\ \frac{\upsilon_{\underline{m}}U_{\underline{m}}R_1-\tau_1L_{\underline{m}}W_1}{\upsilon_{\underline{m}}-\tau_1} & \cdots & \frac{\upsilon_{\underline{m}}U_{\underline{m}}R_{\overline{m}}-\tau_{\overline{m}}L_{\underline{m}}W_{\overline{m}}}{\upsilon_{\underline{m}}-\tau_{\overline{m}}}\end{bmatrix} \tag{2.26}$$

The LMs are complex matrices. In order to get a real macromodel, a similarity transformaion is used as follows [29, 31]

$$\mathbb{L}_R=\mathbb{T}^*\mathbb{L}\mathbb{T},\quad \sigma\mathbb{L}_R=\mathbb{T}^*\sigma\mathbb{L}\mathbb{T}$$

$$\mathbb{U}_R = \mathbb{T}^* \boldsymbol{U}, \quad \mathbb{W}_R = \mathbb{T}\boldsymbol{W} \tag{2.27}$$

where,

$$\mathbb{T} = blkdiag[\mathbb{t}, \ldots, \mathbb{t}] \in \mathbb{C}^{\underline{m} \times \overline{m}}, \quad \mathbb{t} = \frac{1}{\sqrt{2}} \begin{bmatrix} 1 & -j \\ 1 & +j \end{bmatrix}$$

According to [29] state-space realization of the time domain model can be extracted from the regular part of the Loewner Matrix pencil $(s\mathbb{L}_R - \sigma\mathbb{L}_R)$. The regular part is extracted from SVD of $(s\mathbb{L}_R - \sigma\mathbb{L}_R)$. Any value of s can be chosen unless it is not the eigenvalue of $(\mathbb{L}_R, \sigma\mathbb{L}_R)$. Using singular value decomposition (SVD), the realization can be obtained as follows:

$$\begin{gathered} SVD(s\mathbb{L}_R - \sigma\mathbb{L}_R) = \mathbb{Y}\Sigma\mathbb{X}; \\ rank(s\mathbb{L}_R - \sigma\mathbb{L}_R) = rank(\Sigma) = r; \\ \mathbb{Y}_1 \in \mathbb{R}^{\underline{m} \times r} \quad \text{and} \quad \mathbb{X}_1 \in \mathbb{R}^{\overline{m} \times r} \end{gathered} \tag{2.28}$$

Here order or rank of the system is r. Here $\mathbb{Y}$ and $\mathbb{X}$ are left and right eigenvectors. $\mathbb{Y}_1$ and $\mathbb{X}_1$ are constructed from the first r columns of $\mathbb{Y}$ and $\mathbb{X}$. The system matrices are defined as,

$$\begin{gathered} \boldsymbol{E} = \mathbb{Y}_1^* \mathbb{L}_R \mathbb{X}_1; \quad \boldsymbol{A} = \mathbb{Y}_1^* \sigma\mathbb{L}_R \mathbb{X}_1; \\ \boldsymbol{B} = \mathbb{Y}_1^* \mathbb{U}_R; \quad \boldsymbol{C} = -\mathbb{W}_R \mathbb{X}_1; \quad \boldsymbol{D} = 0; \end{gathered} \tag{2.29}$$

At this stage $\boldsymbol{D}$ matrix is always zero. Sometimes embedded $\boldsymbol{D}$ matrix is needed to be extracted to get a stable macromodel as illustrated in [31].

2.6 Circuit Formulation of Distributed Networks

This section illustrates the circuit formulation of distributed electrical networks.

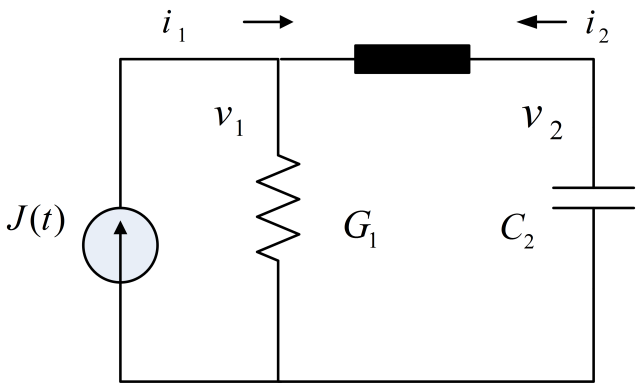

Figure 2.4: Linear Distributed Network

2.6.1 Linear Distributed Networks

Let us consider the linear distributed network shown in Figure 2.4. The Modified Nodal Analysis (MNA) equation can be expressed in time domain as,

$$\begin{bmatrix} G_1 & 0 \\ 0 & 0 \end{bmatrix}\begin{bmatrix} v_1 \\ v_2 \end{bmatrix} + \begin{bmatrix} 0 & 0 \\ 0 & C_2 \end{bmatrix}\begin{bmatrix} \frac{dv_1}{dt} \\ \frac{dv_2}{dt} \end{bmatrix} + \begin{bmatrix} i_1 \\ i_2 \end{bmatrix} = \begin{bmatrix} J(t) \\ 0 \end{bmatrix} \tag{2.30}$$

In the frequency domain, Y-parameter expression of the 2-port distributed network in Figure 2.4 can be expressed as,

$$\begin{bmatrix} I_1 \\ I_2 \end{bmatrix} = \begin{bmatrix} Y_{11} & Y_{12} \\ Y_{21} & Y_{22} \end{bmatrix}\begin{bmatrix} V_1 \\ V_2 \end{bmatrix} \tag{2.31}$$

After macromodeling the distributed network using Loewner modeling, let us consider r elements are present in the port system. In the time domain, following equation (2.21) state space equation for this 2-port system can be written as,

$$\begin{bmatrix} e_{11} & \dots & e_{1r} \\ \vdots & \ddots & \vdots \\ e_{r1} & \dots & e_{rr} \end{bmatrix}\begin{bmatrix} \frac{dx_1}{dt} \\ \vdots \\ \frac{dx_r}{dt} \end{bmatrix} = \begin{bmatrix} a_{11} & \dots & a_{1r} \\ \vdots & \ddots & \vdots \\ a_{r1} & \dots & a_{rr} \end{bmatrix}\begin{bmatrix} x_1 \\ \vdots \\ x_r \end{bmatrix} + \begin{bmatrix} b_{11} & b_{12} \\ \vdots & \vdots \\ b_{r1} & b_{r2} \end{bmatrix}\begin{bmatrix} v_1 \\ v_2 \end{bmatrix} \tag{2.32}$$

$$\begin{bmatrix} i_1 \\ i_2 \end{bmatrix} = \begin{bmatrix} c_{11} & \dots & c_{1r} \\ c_{21} & \dots & c_{2r} \end{bmatrix} \begin{bmatrix} x_1 \\ \vdots \\ x_r \end{bmatrix} + \begin{bmatrix} d_{11} & d_{12} \\ d_{21} & d_{22} \end{bmatrix} \begin{bmatrix} v_1 \\ v_2 \end{bmatrix} \tag{2.33}$$

Now equations (2.32) and (2.33) are embedded in equation (2.30). We first substitute (2.33) into i_1 and i_2 in (2.30). We obtain an equation with parameter $x = [x_1 \dots x_r]$ as,

$$\begin{bmatrix} G_1 + d_{11} & d_{12} & c_{11} & \dots & c_{1r} \\ d_{21} & d_{22} & c_{21} & \dots & c_{2r} \end{bmatrix} \begin{bmatrix} v_1 \\ v_2 \\ x_1 \\ \vdots \\ x_r \end{bmatrix} + \begin{bmatrix} 0 & 0 & 0 & \dots & 0 \\ 0 & C_2 & 0 & \dots & 0 \end{bmatrix} \begin{bmatrix} \frac{dv_1}{dt} \\ \frac{dv_2}{dt} \\ \frac{dx_1}{dt} \\ \vdots \\ \frac{dx_r}{dt} \end{bmatrix} = \begin{bmatrix} J(t) \\ 0 \\ 0 \\ \vdots \\ 0 \end{bmatrix} \tag{2.34}$$

Now we add equation (2.32) to the bottom of equation (2.34). We can get the integrated MNA equation for the whole circuit shown in Figure 2.4 as,

$$\begin{bmatrix} G_1 + d_{11} & d_{12} & c_{11} & \dots & c_{1r} \\ d_{21} & d_{22} & c_{21} & \dots & c_{2r} \\ -b_{11} & -b_{12} & -a_{11} & \dots & -a_{1r} \\ \vdots & \vdots & \vdots & \ddots & \vdots \\ -b_{r1} & -b_{r2} & -a_{r1} & \dots & -a_{rr} \end{bmatrix} \begin{bmatrix} v_1 \\ v_2 \\ x_1 \\ \vdots \\ x_r \end{bmatrix} + \begin{bmatrix} 0 & 0 & 0 & \dots & 0 \\ 0 & C_2 & 0 & \dots & 0 \\ 0 & 0 & e_{11} & \dots & e_{1r} \\ \vdots & \vdots & \vdots & \ddots & \vdots \\ 0 & 0 & e_{r1} & \dots & e_{rr} \end{bmatrix} \begin{bmatrix} \frac{dv_1}{dt} \\ \frac{dv_2}{dt} \\ \frac{dx_1}{dt} \\ \vdots \\ \frac{dx_r}{dt} \end{bmatrix} = \begin{bmatrix} J(t) \\ 0 \\ 0 \\ \vdots \\ 0 \end{bmatrix} \tag{2.35}$$

2.6.2 Nonlinear Distributed Networks

In general, distributed networks in the presence of nonlinear elements can be expressed as [5]

$$C_\phi \frac{dx_\phi(t)}{dt} + G_\phi x_\phi(t) + \sum_{k=1}^{N_t} D_k i_k(t) + F(x_\phi(t)) = b_\phi(t)$$

$$I_k(s) = V_k(s)Y_k(s) \tag{2.36}$$

where

- $x_\phi(t)$ is a vector, which includes node voltages appended by independent and dependent voltage source currents, inductor currents, nonlinear capacitor charge, and nonlinear inductor flux waveform. G_ϕ and C_ϕ are constant matrices describing the lumped memoryless and memory elements of the network, respectively. $b_\phi(t)$ is a vector with entries determined by the independent voltage and current sources. $F(x_\phi(t))$ is a vector describing the nonlinear elements.

- $D_k = [d_{i,j} \in \{0, 1\}]$ is a selector matrix that maps the vector of terminal currents $i_k(t)$ entering the interconnect k into the node space of the circuit network, where $i \in 1, \ldots, \phi$, $j \in 1, \ldots, 2M_k$ and M_k is the number of coupled signal conductors in the kth interconnect. N_t is the number of distributed structures. $Y_k(s)$ is the admittance parameters of interconnect subnetwork in the Laplace domain. $V_k(s)$ and $I_k(s)$ represent the Laplace terminal voltages and currents of interconnect k.

2.6.3 Nonlinear Network

After macromodeling the distributed transmission lines into ODEs, large nonlinear interconnect network can be expressed by,

$$C_\psi \frac{dx(t)}{dt} + G_\psi(t) + F(x(t)) = b(t) \tag{2.37}$$

Here C_ψ matrix contains the admittances for capacitive and inductive elements and G_ψ matrix contains the admittances of resistive and conductive elements. $F(x(t))$ vector comprises the nonlinear elements and x vector represents node voltages and currents flowing through voltage sources and inductors. The vector $b(t)$ contains the values of the independent current sources and independent voltage sources.

2.7 Transient Analysis of Nonlinear Network

The time domain solution of (2.37) is derived by converting the nonlinear differential equations to nonlinear algebraic equations using explicit method such as Forward Euler and implicit methods like Backward Euler and Trapezoidal rule. Explicit methods require no matrix inversion making them computationally less expensive than implicit methods that require matrix inversion. But explicit methods are never used for circuit simulation as they are not absolutely stable for all step sizes. On the other hand, implicit methods are absolutely stable and used for solving nonlinear circuits with Newton-Raphson iteration at each time step. For multinode network after using Trapezoidal rule difference equation of (2.37) can be written as

$$(\frac{C_\psi}{\Delta t} + \frac{G_\psi}{2})x_{t+1} + \frac{F(x_{t+1})}{2} - (\frac{C_\psi}{\Delta t} - \frac{G_\psi}{2})x_t + \frac{F(x_t)}{2} = \frac{b_t + b_{t+1}}{2} \tag{2.38}$$

Here Δt is the step size. Let us consider step size Δt is very small and does not change during time domain simulation.

After applying Newton-Raphson method the problem becomes solving the following function,

$$f_{t+1}^k = (\frac{C_\psi}{\Delta t} + \frac{G_\psi}{2})x_{t+1} + \frac{F(x_{t+1})}{2} - (\frac{C_\psi}{\Delta t} - \frac{G_\psi}{2})x_t + \frac{F(x_t)}{2} - \frac{b_t + b_{t+1}}{2} = 0 \tag{2.39}$$

where x_{t+1} is the unknown vector with n number of variables to be solved at each iteration by applying,

$$x_{t+1}^{k+1} = x_{t+1}^k + \Delta x_{t+1}^k \tag{2.40}$$

$$\Delta x_{t+1}^k = -(\mathbb{M}_{t+1}^k)^{-1} f_{t+1}^k \tag{2.41}$$

where k is the iteration number. Here $\mathbb{M}$ is an $n \times n$ Jacobian matrix and can be expressed as,

$$\mathbb{M}_{t+1}^k = (\frac{C_\psi}{\Delta t} + \frac{G_\psi}{2}) + \frac{1}{2}\frac{dF(x_{t+1}^k)}{dx_{t+1}} \tag{2.42}$$

The most costly matrix calculation at each step of Newton iteration is solving the inverse of

the Jacobian matrix in equation (2.42). Each iteration costs one LU factorization and one forward/backward substitution.

In the Jacobian matrix, C_ψ and G_ψ are very large matrices. To invert the Jacobian matrix at each step of Newton iteration becomes a CPU intensive task for time domain analysis. This issue has been addressed in this thesis.

2.8 Conclusion

In this chapter, an overview of different macromodeling techniques of interconnect is given based on known and unknown physical characteristics of the structures. Furthermore, MNA equations are derived for Loewner matrix modeling technique. Finally, a brief review of non-linear circuit analysis algorithm is presented.

Chapter 3

Noisy Data Iterative Loewner Macromodeling

3.1 Introduction

System identification has become a challenging task for high speed devices and structures. To identify a system without any prior knowledge of physical characteristics is based on frequency domain tabulated data. Recently Loewner Matrix (LM) [29–31] based method was proposed to generate state-space macromodels from frequency domain measured data. This method faces difficulty to identify a system accurately from contaminated noisy frequency data [36]. This chapter presents an iterative method to macromodel a system from frequency data contaminated by noise based on Loewner Matrix framework. In this proposed algorithm, eigenvectors are generated from previous Loewner Matrix approximated model. As previous approximated model has less noise in it than the original data, it is illustrated that this method will give better approximation of Loewner matrix method thus improving the accuracy of the approximated Loewner matrix model. Numerical examples are provided to demonstrate the validity and accuracy of the proposed method.

3.2 LM for Noisy Frequency Responses

A single port or a multiport network can be characterized by measured data in the form of admittance, impedance, hybrid or scattering parameter data. Let us consider that the frequency domain scattering (S-parameter) or admittance (Y-parameter) data can be expressed as,

$$\begin{gathered}\{s_m, \boldsymbol{Y}(s_m)\} \\ \boldsymbol{Y}(s_m) = [Y_{ij}(s_m)] \quad (i, j \in 1, ..., P)\end{gathered} \tag{3.1}$$

where, s_m is the complex frequency, $\boldsymbol{Y}(s_m)$ is the S-parameter or Y-parameter data at frequency s_m, $m = 1, 2, \ldots, M$, where M is the number of data points and P is the number of ports of the network. Let us consider the frequency domain noisy data as,

$$\tilde{\boldsymbol{Y}}(s_m) = \boldsymbol{Y}(s_m) + \epsilon(s_m) \tag{3.2}$$

Here $\tilde{\boldsymbol{Y}}$ is the contaminated data and ϵ is a zero-mean random noise (meaning the expected mean value $E[\epsilon]$ is zero).

From noisy data set $\{s_m, \tilde{\boldsymbol{Y}}(s_m)\}$, using equation (2.24) right and left noisy complex data matrices $\tilde{\boldsymbol{W}}$ and $\tilde{\boldsymbol{U}}$ are created respectively and can be expressed as,

$$\begin{aligned}\tilde{\boldsymbol{W}} &= \boldsymbol{W} + \mathbb{H}^{\boldsymbol{W}_\epsilon} \\ \tilde{\boldsymbol{U}} &= \boldsymbol{U} + \mathbb{H}^{\boldsymbol{U}_\epsilon}\end{aligned} \tag{3.3}$$

Here $\mathbb{H}^{\boldsymbol{W}_\epsilon}$ and $\mathbb{H}^{\boldsymbol{U}_\epsilon}$ are due to noise ϵ in the data. As ϵ is a zero mean randon noise, the expected mean values of $\mathbb{H}^{\boldsymbol{W}_\epsilon}$ and $\mathbb{H}^{\boldsymbol{U}_\epsilon}$ are zero.

$$\begin{aligned}E[\mathbb{H}^{\boldsymbol{W}_\epsilon}] &= 0 \\ E[\mathbb{H}^{\boldsymbol{U}_\epsilon}] &= 0\end{aligned} \tag{3.4}$$

From noisy complex $\tilde{\boldsymbol{W}}$ and $\tilde{\boldsymbol{U}}$ matrices following equation (2.25) to (2.27) $\tilde{\mathbb{W}}_R$, $\tilde{\mathbb{U}}_R$, $\tilde{\mathbb{L}}_R$, $\sigma\tilde{\mathbb{L}}_R$

matrices are created and can be expressed as,

$$\begin{aligned}\tilde{\mathbb{W}}_R &= \mathbb{W}_R + \mathbb{H}^{\mathbb{W}_{R\epsilon}} \\ \tilde{\mathbb{U}}_R &= \mathbb{U}_R + \mathbb{H}^{\mathbb{U}_{R\epsilon}} \\ \tilde{\mathbb{L}}_R &= \mathbb{L}_R + \mathbb{H}^{\mathbb{U}_{R\epsilon}} + \mathbb{H}^{\mathbb{W}_{R\epsilon}} \\ \sigma\tilde{\mathbb{L}}_R &= \sigma\mathbb{L}_R + \mathbb{H}^{\mathbb{U}_{R\epsilon}} + \mathbb{H}^{\mathbb{W}_{R\epsilon}}\end{aligned} \tag{3.5}$$

Here $\tilde{\mathbb{W}}_R$, $\tilde{\mathbb{U}}_R$, $\tilde{\mathbb{L}}_R$, $\sigma\tilde{\mathbb{L}}_R$ are real right data noisy matrix, real left data noisy matrix, real noisy Loewner matrix and real noisy shifted Loewner matrix from given noisy data respectively. $\mathbb{H}^{\mathbb{W}_{R\epsilon}}$ and $\mathbb{H}^{\mathbb{U}_{R\epsilon}}$ comes from the noisy data matrices $\tilde{\boldsymbol{W}}$ and $\tilde{\boldsymbol{U}}$, respectively. Since expected mean value $E[\epsilon]$ is zero, expected mean values of $\mathbb{H}^{\mathbb{W}_{R\epsilon}}$ and $\mathbb{H}^{\mathbb{U}_{R\epsilon}}$ are also zero.

$$\begin{aligned}E[\mathbb{H}^{\mathbb{W}_{R\epsilon}}] &= 0 \\ E[\mathbb{H}^{\mathbb{U}_{R\epsilon}}] &= 0\end{aligned} \tag{3.6}$$

$\mathbb{H}^{\mathbb{W}_{R\epsilon}}$ and $\mathbb{H}^{\mathbb{U}_{R\epsilon}}$ matrices do not statistically bias the results of LM approximation. However, Singular Value Decomposition (SVD) of Loewner Matrix and shifted Loewner Matrix is pertubed as bellow,

$$SVD(s\tilde{\mathbb{L}}_R - \sigma\tilde{\mathbb{L}}_R) = \tilde{\mathbb{Y}}\tilde{\mathbf{\Sigma}}\tilde{\mathbb{X}}; \tag{3.7}$$

For different example perturbation of SVD of Loewner matrices is different. SVD of noisy Loewner Matrices of Example 2 & 3 (which are described later in Chapter 3) are given in Figure 3.1 & 3.2, respectively. In these figures different noise values are added to frequency domain data to see the change of SVD of Loewner matrices. As a result, from equation (3.7) left and right eigenvectors $\tilde{\mathbb{Y}}$ and $\tilde{\mathbb{X}}$, respectively, has noise in it.

$\tilde{\mathbb{Y}}$ and $\tilde{\mathbb{X}}$ are noisy left and right eigenvectors. $\tilde{\mathbb{Y}}_1$ and $\tilde{\mathbb{X}}_1$ are constructed from the first r columns of $\tilde{\mathbb{Y}}$ and $\tilde{\mathbb{X}}$.

$$\begin{aligned}\tilde{\mathbb{Y}}_1 &= \mathbb{Y}_1 + \mathbb{Y}_1^{\mathbb{U}_{R\epsilon}} + \mathbb{Y}_1^{\mathbb{W}_{R\epsilon}} \\ \tilde{\mathbb{X}}_1 &= \mathbb{X}_1 + \mathbb{X}_1^{\mathbb{U}_{R\epsilon}} + \mathbb{X}_1^{\mathbb{W}_{R\epsilon}}\end{aligned} \tag{3.8}$$

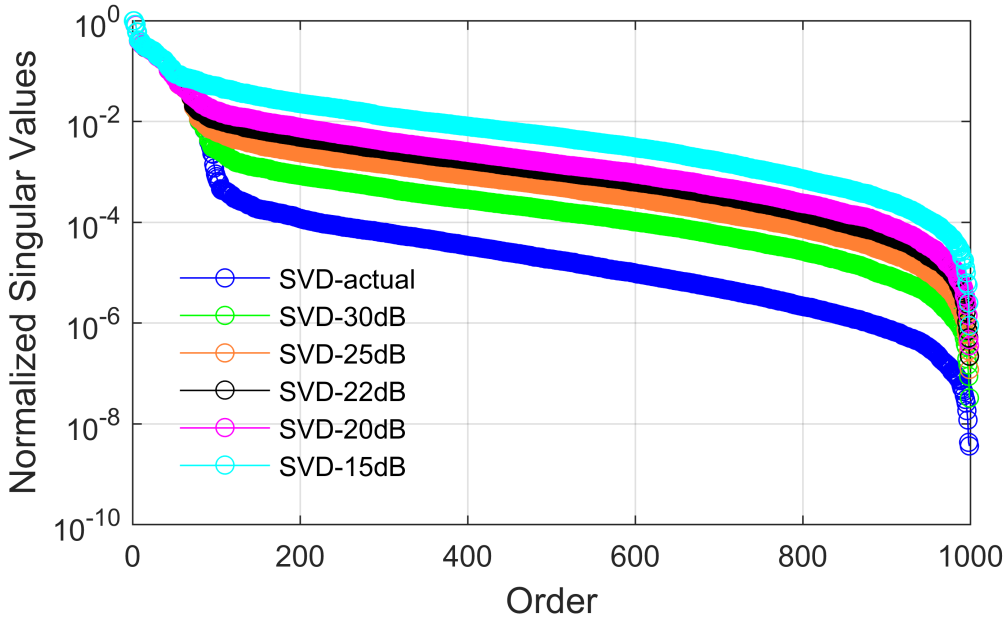

Figure 3.1: Normalized Singular Values (Example 2).

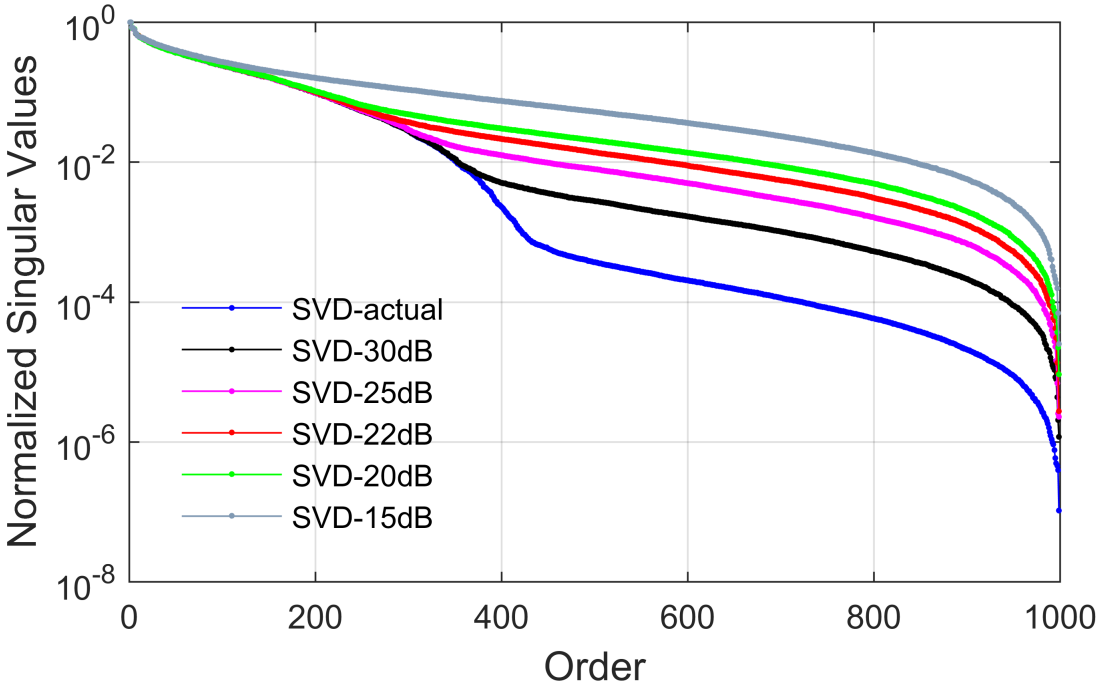

Figure 3.2: Normalized Singular Values (Example 3).

Here $\mathbb{Y}_1^{\mathbb{U}_{R\epsilon}}$, $\mathbb{Y}_1^{\mathbb{W}_{R\epsilon}}$, $\mathbb{X}_1^{\mathbb{U}_{R\epsilon}}$ and $\mathbb{X}_1^{\mathbb{W}_{R\epsilon}}$ are noise terms. When we constructed $\tilde{\mathbb{Y}}_1$ and $\tilde{\mathbb{X}}_1$ from the first r columns of $\tilde{\mathbb{Y}}$ and $\tilde{\mathbb{X}}$, we eliminate most of the noisy parts from $\tilde{\mathbb{Y}}$ and $\tilde{\mathbb{X}}$ matrices. As a result, expected mean value of $\mathbb{Y}_1^{\mathbb{U}_{R\epsilon}}$, $\mathbb{Y}_1^{\mathbb{W}_{R\epsilon}}$, $\mathbb{X}_1^{\mathbb{U}_{R\epsilon}}$ and $\mathbb{X}_1^{\mathbb{W}_{R\epsilon}}$ matrices are not equal to zero.

The matrices recovered from the noisy data are perturbed from the original values because of $\mathbb{Y}_1^{\mathbb{U}_{R\epsilon}}$, $\mathbb{Y}_1^{\mathbb{W}_{R\epsilon}}$, $\mathbb{X}_1^{\mathbb{U}_{R\epsilon}}$ and $\mathbb{X}_1^{\mathbb{W}_{R\epsilon}}$ matrices. As a result, the realization $\boldsymbol{E}, \boldsymbol{A}, \boldsymbol{B}, \boldsymbol{C}$ are perturbed by the noisy data and the noisy realization becomes following equation (2.29) as,

$$\begin{aligned}
\tilde{E} &= \tilde{\mathbb{Y}}_1^{*}\tilde{\mathbb{L}}_R\tilde{\mathbb{X}}_1 = \boldsymbol{E} + \boldsymbol{E_n};\\
\tilde{A} &= \tilde{\mathbb{Y}}_1^{*}\sigma\tilde{\mathbb{L}}_R\tilde{\mathbb{X}}_1 = \boldsymbol{A} + \boldsymbol{A_n};\\
\tilde{B} &= \tilde{\mathbb{Y}}_1^{*}\tilde{\mathbb{U}}_R = \boldsymbol{B} + \boldsymbol{B_n};\\
\tilde{C} &= -\tilde{\mathbb{W}}_R\tilde{\mathbb{X}}_1 = \boldsymbol{C} + \boldsymbol{C_n};
\end{aligned} \tag{3.9}$$

Here $\boldsymbol{E_n}$, $\boldsymbol{A_n}$, $\boldsymbol{B_n}$ and $\boldsymbol{C_n}$ are noise parts in the realization due to $\mathbb{Y}_1^{\mathbb{U}_{R\epsilon}}$, $\mathbb{Y}_1^{\mathbb{W}_{R\epsilon}}$, $\mathbb{X}_1^{\mathbb{U}_{R\epsilon}}$ and $\mathbb{X}_1^{\mathbb{W}_{R\epsilon}}$ matrices. Following section describes an approach to reduce this noise in the realization to improve the accuracy of LM approximation.

3.3 Proposed Algorithm

3.3.1 Eigenvector Correction from Noise-free Data

Let us see what happens if we use the eigenvectors $\mathbb{Y}_1$ and $\mathbb{X}_1$ from the actual (noise-free) data and data matrices ($\tilde{\mathbb{W}}_R$, $\tilde{\mathbb{U}}_R$, $\tilde{\mathbb{L}}_R$, $\sigma\tilde{\mathbb{L}}_R$) from the noisy data. In this case, our realization becomes,

$$\begin{aligned}
\grave{E} &= \mathbb{Y}_1^{*}\tilde{\mathbb{L}}_R\mathbb{X}_1;\\
\grave{A} &= \mathbb{Y}_1^{*}\sigma\tilde{\mathbb{L}}_R\mathbb{X}_1;\\
\grave{B} &= \mathbb{Y}_1^{*}\tilde{\mathbb{U}}_R;\\
\grave{C} &= -\tilde{\mathbb{W}}_R\mathbb{X}_1;
\end{aligned} \tag{3.10}$$

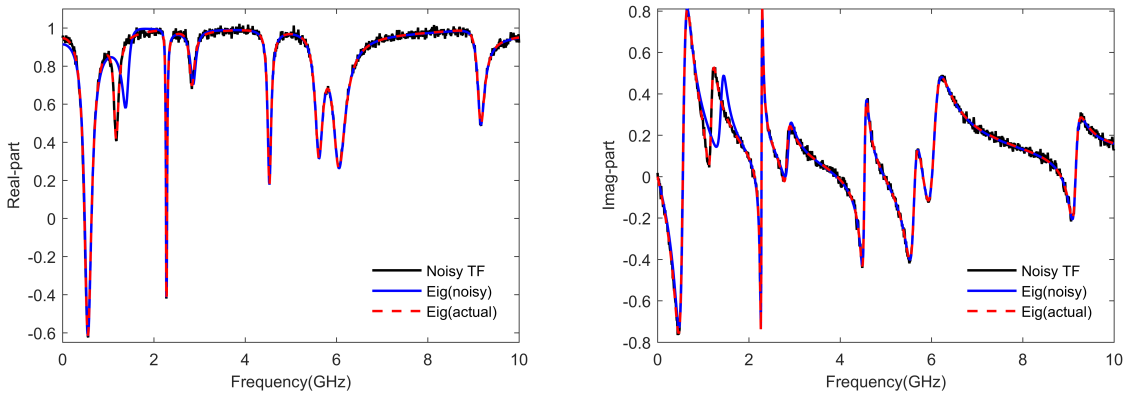

(a) (b)

Figure 3.3: Rational Approximation of the 18-dB SNR data using Noisy Eigenvectors (blue) and Actual (Noise-free) Eigenvectors (red). (a) Real part and (b) Imaginary part plots (Example 1).

This realization is different from equation (3.9). From Figure 3.3, we can see two approximations, one by using eigenvectors from the actual (noise-free) data and other one from noisy data. We can get a better approximation of the LM model by using eigenvectors from actual data. As mentioned above, noise part in $\tilde{\mathbb{W}}_R$, $\tilde{\mathbb{U}}_R$, $\tilde{\mathbb{L}}_R$, $\sigma\tilde{\mathbb{L}}_R$ matrices have expected mean values of zero due to noise ϵ, these matrices do not statistically bias the results of LM approximation.

3.3.2 Eigenvector Correction from Noisy Data

In reality we do not have the noise free data to get the actual eigenvectors. Thus we are proposing an algorithm to use the eigenvectors from previous Loewner method approximated data to reduce the noise in the eigenvectors. Though this data is biased, it has comparatively less noise in it after first approximation. As a result, Loewner and shifted Loewner matrices formed by approximated data will have less noise in them. As eigenvectors are too sensitive to SVD change of Loewner matrices, eigenvectors created from approximated data is closer to the actual or noise-free eigenvectors. We are using an iterative approach to have these less noisy eigenvectors from previous approximation. Consequently, we can get a better approximation of the macromodel from the measured noisy data. Here the proposed method has been described.

Algorithm 1 Update eigenvectors from previous LM approximated data for order r

Given: $\{\tilde{\boldsymbol{Y}}(s_m), s_m\}$ where $\tilde{\boldsymbol{Y}}(s_m)$ are the measured parameters at frequency $f_m = \frac{s_m}{2\pi}$
Output: $\hat{E}$, $\hat{A}$, $\hat{B}$, $\hat{C}$ model of the system.

1: $\{\tilde{\boldsymbol{Y}}(s_m), s_m\} \rightarrow$ Construct $\tilde{\mathbb{L}}_R, \sigma\tilde{\mathbb{L}}_R, \tilde{\mathbb{W}}_R, \tilde{\mathbb{U}}_R$ using (2.24)-(2.27)
2: $[\tilde{\mathbb{Y}}, \tilde{\boldsymbol{\Sigma}}, \tilde{\mathbb{X}}]$=svd$(s\tilde{\mathbb{L}}_R - \sigma\tilde{\mathbb{L}}_R)$.
3: $\tilde{\mathbb{Y}}_1 = \tilde{\mathbb{Y}}(:, 1:r)$, $\tilde{\mathbb{X}}_1 = \tilde{\mathbb{X}}(:, 1:r)$.
4: $\tilde{E} \leftarrow \tilde{\mathbb{Y}}_1^* \tilde{\mathbb{L}}_R \tilde{\mathbb{X}}_1, \tilde{A} \leftarrow \tilde{\mathbb{Y}}_1^* \sigma\tilde{\mathbb{L}}_R \tilde{\mathbb{X}}_1, \tilde{B} \leftarrow \tilde{\mathbb{Y}}_1^* \tilde{\mathbb{U}}_R, \tilde{C} \leftarrow -\tilde{\mathbb{W}}_R \tilde{\mathbb{X}}_1$.
5: $\tilde{\boldsymbol{Y}}_{\mathbf{1}}(s) \leftarrow \tilde{C}(s\tilde{E} - \tilde{A})^{-1}\tilde{B}$
6: $\{\tilde{\boldsymbol{Y}}_1(s_m), s_m\} \rightarrow$ Construct $\mathbb{L}_{R\Psi}, \sigma\mathbb{L}_{R\Psi}, \mathbb{W}_{R\Psi}, \mathbb{U}_{R\Psi}$ using (2.24)-(2.27)
7: $[\mathbb{Y}_\Psi, \boldsymbol{\Sigma}_\Psi, \mathbb{X}_\Psi]$=svd$(s\mathbb{L}_{R\Psi} - \sigma\mathbb{L}_{R\Psi})$.
8: $\mathbb{Y}_{\Psi 1} = \mathbb{Y}_\Psi(:, 1:r)$, $\mathbb{X}_{\Psi 1} = \mathbb{X}_\Psi(:, 1:r)$.
9: $\hat{E} \leftarrow \mathbb{Y}_{\Psi 1}^* \tilde{\mathbb{L}}_R \mathbb{X}_{\Psi 1}, \hat{A} \leftarrow \mathbb{Y}_{\Psi 1}^* \sigma\tilde{\mathbb{L}}_R \mathbb{X}_{\Psi 1}, \ \hat{B} \leftarrow \mathbb{Y}_{\Psi 1}^* \tilde{\mathbb{U}}_R, \ \hat{C} \leftarrow -\tilde{\mathbb{W}}_R \mathbb{X}_{\Psi 1}$.
10: $\tilde{\boldsymbol{Y}}_{\mathbf{2}}(s) = \hat{C}(s\hat{E} - \hat{A})^{-1}\hat{B}$
11: Update $\tilde{\boldsymbol{Y}}_{\mathbf{1}}(s) \leftarrow \tilde{\boldsymbol{Y}}_{\mathbf{2}}(s)$, goto step 6 and repeat 6-11 until convergence.
12: Update $\tilde{\boldsymbol{Y}}_{\mathbf{1}}(s) \leftarrow \tilde{\boldsymbol{Y}}_{\mathbf{2}}(s)$, goto step 6 and repeat 6-9 to get the output Loewner model matrices.

3.3.3 Description of Proposed Method with LM

After the first approximation, we got $\tilde{E}$, $\tilde{A}$, $\tilde{B}$ and $\tilde{C}$ matrices mentioned in equation (3.9). Then we create our first approximated data as,

$$\tilde{\boldsymbol{Y}}_{\mathbf{1}}(s) = \tilde{C}(s\tilde{E} - \tilde{A})^{-1}\tilde{B} \tag{3.11}$$

Our first approximated data becomes,

$$\tilde{\boldsymbol{Y}}_{\mathbf{1}}(s_m) = \boldsymbol{Y}(s_m) + \Psi(s_m) \tag{3.12}$$

where Ψ is the error in the first approximation of noisy data $\tilde{\boldsymbol{Y}}(s)$. Here Ψ is less noisy than ϵ and Ψ is not zero-mean random noise (meaning expected mean value is not equal to zero as $E[\Psi] \neq 0$)

Using this first approximated data, $\tilde{\boldsymbol{Y}}_{\mathbf{1}}$ using equation (2.24) we construct complex right data

matrix $\tilde{\boldsymbol{W}}_\Psi$ and complex left data matrix $\tilde{\boldsymbol{U}}_\Psi$. They are expressed as,

$$\begin{aligned} \tilde{\boldsymbol{W}}_\Psi &= \boldsymbol{W} + \mathbb{H}^{\boldsymbol{W}_\Psi} \\ \tilde{\boldsymbol{U}}_\Psi &= \boldsymbol{U} + \mathbb{H}^{\boldsymbol{U}_\Psi} \end{aligned} \tag{3.13}$$

$\mathbb{H}^{\boldsymbol{W}_\Psi}$ and $\mathbb{H}^{\boldsymbol{U}_\Psi}$ are noise terms due to Ψ in first approximated data $\tilde{\boldsymbol{Y}}_{\mathbf{1}}$. Expected mean values of $\mathbb{H}^{\boldsymbol{W}_\Psi}$ and $\mathbb{H}^{\boldsymbol{U}_\Psi}$ are not zero as Ψ is not zero-mean randon noise.

$$\begin{aligned} E[\mathbb{H}^{\boldsymbol{W}_\Psi}] \neq 0 \\ E[\mathbb{H}^{\boldsymbol{W}_\Psi}] \neq 0 \end{aligned} \tag{3.14}$$

From $\tilde{\boldsymbol{W}}_\Psi$ and $\tilde{\boldsymbol{U}}_\Psi$ matrices we create $\mathbb{W}_{R\Psi}$, $\mathbb{U}_{R\Psi}$, $\mathbb{L}_{R\Psi}$ and $\sigma\mathbb{L}_{R\Psi}$ matrices following equation (2.25) to (2.27) and can be expressed as,

$$\begin{aligned} \mathbb{W}_{R\Psi} &= \mathbb{W}_R + \mathbb{H}^{\mathbb{W}_{R\Psi}} \\ \mathbb{U}_{R\Psi} &= \mathbb{U}_R + \mathbb{H}^{\mathbb{U}_{R\Psi}} \\ \mathbb{L}_{R\Psi} &= \mathbb{L}_R + \mathbb{H}^{\mathbb{U}_{R\Psi}} + \mathbb{H}^{\mathbb{W}_{R\Psi}} \\ \sigma\mathbb{L}_{R\Psi} &= \sigma\mathbb{L}_R + \mathbb{H}^{\mathbb{U}_{R\Psi}} + \mathbb{H}^{\mathbb{W}_{R\Psi}} \end{aligned} \tag{3.15}$$

Here $\mathbb{W}_{R\Psi}$, $\mathbb{U}_{R\Psi}$, $\mathbb{L}_{R\Psi}$ and $\sigma\mathbb{L}_{R\Psi}$ matrices are real right data biased matrix, real left data biased matrix, real biased Loewner matrix and real biased shifted Loewner matrix, respectively. Here $\mathbb{H}^{\mathbb{W}_{R\Psi}}$ and $\mathbb{H}^{\mathbb{U}_{R\Psi}}$ matrices are the biased terms. Expected mean values of $\mathbb{H}^{\mathbb{W}_{R\Psi}}$ and $\mathbb{H}^{\mathbb{U}_{R\Psi}}$ are also not zero because Ψ is not a zero-mean randon noise.

$$\begin{aligned} E[\mathbb{H}^{\mathbb{W}_{R\Psi}}] \neq 0 \\ E[\mathbb{H}^{\mathbb{U}_{R\Psi}}] \neq 0 \end{aligned} \tag{3.16}$$

The expected mean values of the biased terms present in $\mathbb{W}_{R\Psi}$, $\mathbb{U}_{R\Psi}$, $\mathbb{L}_{R\Psi}$ and $\sigma\mathbb{L}_{R\Psi}$ matrices are not zero as Ψ is not a zero-mean random noise. So, these matrices are biased. As a result, they were not used for our second approximation. Instead $\tilde{\mathbb{W}}_R$, $\tilde{\mathbb{U}}_R$, $\tilde{\mathbb{L}}_R$, $\sigma\tilde{\mathbb{L}}_R$ matrices are used

from equation (3.5) due to zero-mean random noise ϵ terms present in them. However, $\mathbb{L}_{R\Psi}$ and $\sigma\mathbb{L}_{R\Psi}$ matrices were used to get less noisy eigenvectors, because they have less noise due to noise Ψ.

From the SVD of $(s\mathbb{L}_{R\Psi} - \sigma\mathbb{L}_{R\Psi})$ matrix we get $\mathbb{Y}_\Psi$ & $\mathbb{X}_\Psi$ matrices.

$$SVD\,(s\mathbb{L}_{R\Psi} - \sigma\mathbb{L}_{R\Psi}) = \mathbb{Y}_\Psi \Sigma_\Psi \mathbb{X}_\Psi \tag{3.17}$$

$\mathbb{Y}_\Psi$ & $\mathbb{X}_\Psi$ are left and right noisy eigenvectors of the first approximated data. From the first r columns of $\mathbb{Y}_\Psi$ & $\mathbb{X}_\Psi$, we create $\mathbb{Y}_{\Psi 1}$ and $\mathbb{X}_{\Psi 1}$ matrices as,

$$\begin{aligned} \mathbb{Y}_{\Psi 1} &= \mathbb{Y}_1 + \mathbb{Y}_1^{\mathbb{U}_{R\Psi}} + \mathbb{Y}_1^{\mathbb{W}_{R\Psi}} \\ \mathbb{X}_{\Psi 1} &= \mathbb{X}_1 + \mathbb{X}_1^{\mathbb{U}_{R\Psi}} + \mathbb{X}_1^{\mathbb{W}_{R\Psi}} \end{aligned} \tag{3.18}$$

Here $\mathbb{Y}_1^{\mathbb{U}_{R\Psi}}$, $\mathbb{Y}_1^{\mathbb{W}_{R\Psi}}$, $\mathbb{X}_1^{\mathbb{U}_{R\Psi}}$ and $\mathbb{X}_1^{\mathbb{W}_{R\Psi}}$ matrices are noise terms and expected mean values of these matrices are not zero.

Again $\mathbb{Y}_1^{\mathbb{U}_{R\Psi}}$, $\mathbb{Y}_1^{\mathbb{W}_{R\Psi}}$, $\mathbb{X}_1^{\mathbb{U}_{R\Psi}}$ and $\mathbb{X}_1^{\mathbb{W}_{R\Psi}}$ matrices are less noisy than $\mathbb{Y}_1^{\mathbb{U}_{R\epsilon}}$, $\mathbb{Y}_1^{\mathbb{W}_{R\epsilon}}$, $\mathbb{X}_1^{\mathbb{U}_{R\epsilon}}$ and $\mathbb{X}_1^{\mathbb{W}_{R\epsilon}}$ matrices because Ψ has less noise in it than ϵ. As a result, $\mathbb{Y}_{\Psi 1}$ and $\mathbb{X}_{\Psi 1}$ eigenvectors have less noise in it than $\tilde{\mathbb{Y}}_1$ and $\tilde{\mathbb{X}}_1$ eigenvectors. Therefore, for our second approximation we use $\mathbb{Y}_{\Psi 1}$ and $\mathbb{X}_{\Psi 1}$ eigenvectors instead of $\tilde{\mathbb{Y}}_1$ and $\tilde{\mathbb{X}}_1$ eigenvectors. The realization of matrices using eigenvectors from first approximated data can be defined as,

$$\begin{aligned} \hat{E} &= \mathbb{Y}_{\Psi 1}^* \tilde{\mathbb{L}}_R \mathbb{X}_{\Psi 1}; \\ \hat{A} &= \mathbb{Y}_{\Psi 1}^* \sigma\tilde{\mathbb{L}}_R \mathbb{X}_{\Psi 1}; \\ \hat{B} &= \mathbb{Y}_{\Psi 1}^* \tilde{\mathbb{U}}_R; \\ \hat{C} &= -\tilde{\mathbb{W}}_R \mathbb{X}_{\Psi 1}; \end{aligned} \tag{3.19}$$

Using these matrices from equation (3.19) we get our second approximation as,

$$\tilde{\boldsymbol{Y}}_{\boldsymbol{2}}(s) = \hat{C}(s\hat{E} - \hat{A})^{-1}\hat{B} \tag{3.20}$$

To make an iteration of this method, we update the data value of $\tilde{\boldsymbol{Y}}_1(s)$ from $\tilde{\boldsymbol{Y}}_2(s)$ data and repeat this method for a selected order until convergence. This proposed approach will yield more accurate result than LM solution of (3.11).

3.3.4 Methodology to Construct Previous Approximations with LM

Algorithm 1 describes the procedure to construct the less noisy eigenvectors to remove noise from the measured data and the procedure to extract a model from the given data.

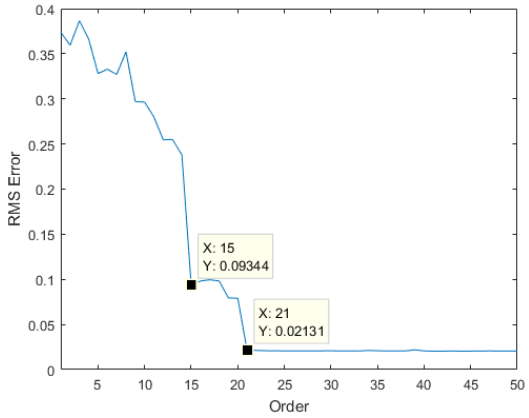

Figure 3.4: RMS error vs. order (Example 1) SNR=18dB

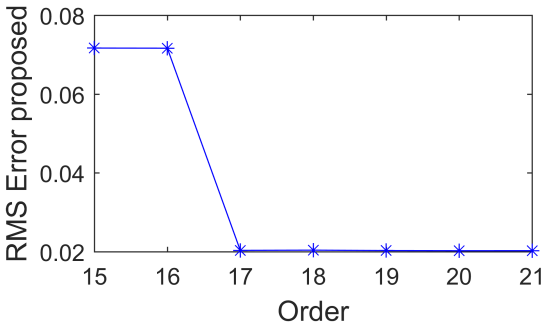

Figure 3.5: Proposed RMS error vs. order (Example 1) SNR=18dB.

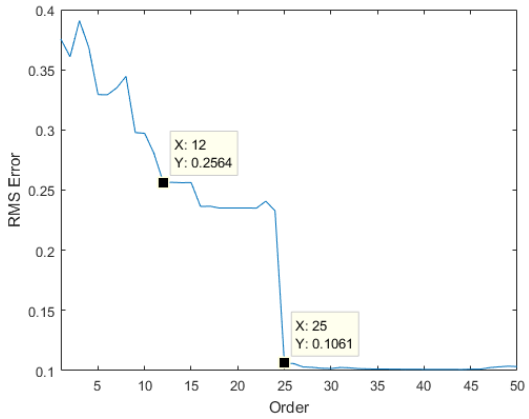

Figure 3.6: RMS error vs. order (Example 1) SNR=16dB.

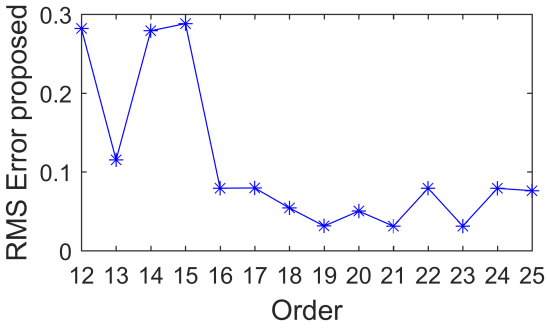

Figure 3.7: Proposed RMS error vs. order (Example 1) SNR=16dB.

3.3.5 Order Selection

In Loewner Matrix modeling, an order is selected for model order reduction of the system. This order of the system can be identified from the Singular Value Decomposition (SVD) drop of Loewner Matrix [29]. When there is noise present in the data, SVD of the Loewner matrices is contaminated and order of the system is hard to calculate from the SVD drop of LM. Therefore, we have used LM approximated model RMS error / H_2 error vs. order as our reference graph to select the order of the system. From LM approximated model RMS error / H_2 error vs. order graph we pick a range of orders. In case of Example 1 the range is from 15 to 21 shown in Figure 3.4 for SNR=18 dB. Then for all these orders we apply our proposed algorithm. From Figure 3.5, representing proposed RMS error vs. order graph, we can see for order 17 the error is lowest. And thus order 17 was chosen for Example 1 in case of SNR=18dB. For SNR=16dB the range of order is selected from 12 to 25 in Figure 3.6 showing LM approximated model RMS error vs. order of the system. After applying our proposed algorithm for these range of order values, the lowest error occurred at order 19 shown in Figure 3.7.

3.4 Numerical Examples

Four numerical examples are provided in this section to demonstrate the accuracy of the proposed iterative LM method for the noisy frequency data. In the controlled experiments ϵ is the added random noise [12, 17] and is defined as,

$$\epsilon(s_m) = \boldsymbol{Y}(s_m) \times 10^{-SNR/10} \times (\boldsymbol{N}_r + j\boldsymbol{N}_i) \tag{3.21}$$

Here $\boldsymbol{N}_r$ & $\boldsymbol{N}_i$ are real and imaginary random Gaussian noise. The noise level can be changed by adjusting the Signal to Noise Ratio (SNR).

Table 3.1: Poles and Residues of the TF (Example 1)

Poles (GHz) (p^k)	Residues (GHz) (r^k)
-0.6132 ± 3.4551i	-0.9877 ∓ 0.0809i
-0.3940 ± 7.3758i	-0.2067 ∓ 0.0131i
-0.0880 ± 14.3024i	-0.1382 ∓ 0.0145i
-0.4097 ± 17.7864i	-0.1182 ∓ 0.0166i
-0.2991 ± 28.4622i	-0.2426 ∓ 0.0145i
-0.6447 ± 35.2669i	-0.4043 ∓ 0.0297i
-1.0135 ± 37.9655i	-0.6787 ∓ 0.1465i
-0.5711 ± 57.4748i	-0.2626 ∓ 0.1037i
d=0.980	

3.4.1 Example 1

The first example is a synthetic transfer function (TF) with 16 poles are described in Table 3.1 is from [35]. Here 18 dB and 16 dB signal-to-noise ratios (SNRs) are considered.

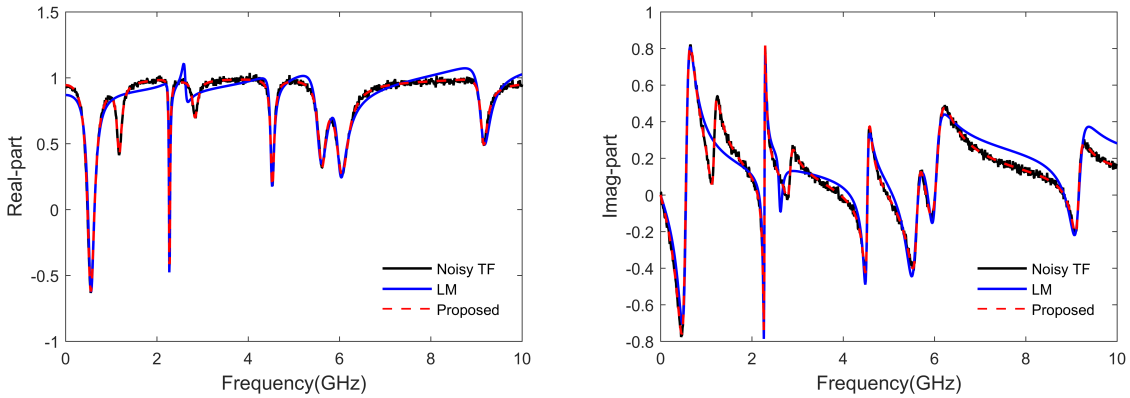

(a) (b)

Figure 3.8: Rational Approximation of the 18-dB SNR data using LM and LM-Proposed approximation. (a) Real part and (b) Imaginary part plots (Example 1).

Case 1:

Figure 3.8 shows the sample response of the TF with 18 dB SNR, TF from Loewner modeling and proposed LM method using 1000 sample points distributed evenly between 0-10 GHz.

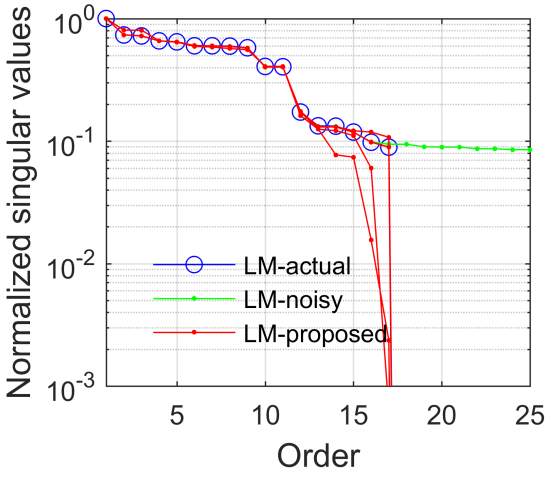

Figure 3.9: Normalized SVD versus Order (Example 1).

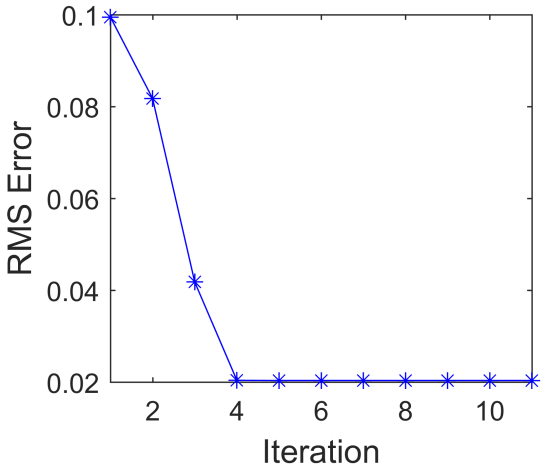

Figure 3.10: RMS error vs. iteration count for SNR= 18 dB (Example 1).

The LM algorithm is not able to catch the poles of the system due to biasing from the model approximation, while the proposed method to use the eigenvectors from the previous approximation iteratively shows good agreement with the original TF. Here order was found 17 to approximate the previous LM model.

The SVD of actual (noise-free) data, noisy data and proposed method data are shown in Figure 3.9. Figure 3.10 shows the root mean square (rms) error versus iteration number, calculated as

$$RMS\ error = \sqrt{\frac{1}{N_s}\sum_{j=1}^{N_s} \|Y(s_j) - Y_{app}(s_j)\|^2} \tag{3.22}$$

where $Y(s_j)$ is equal to noisy TF and $Y_{app}(s_j)$ corresponds to approximated TF. The rms error for LM is 0.1032, while the rms error of LM-proposed is 0.01991 at tenth iteration.

Table 3.2 shows that the proposed iterative algorithm matches the poles of the original system to within 0.0764%, while LM algorithm missed the pole at -0.3940 ± 7.3758. Figure 3.11 illustrates logarithmic RMS error vs. frequency plots for actual (noise-free) data LM approximation, noisy data LM approximation and noisy data proposed LM approximation.

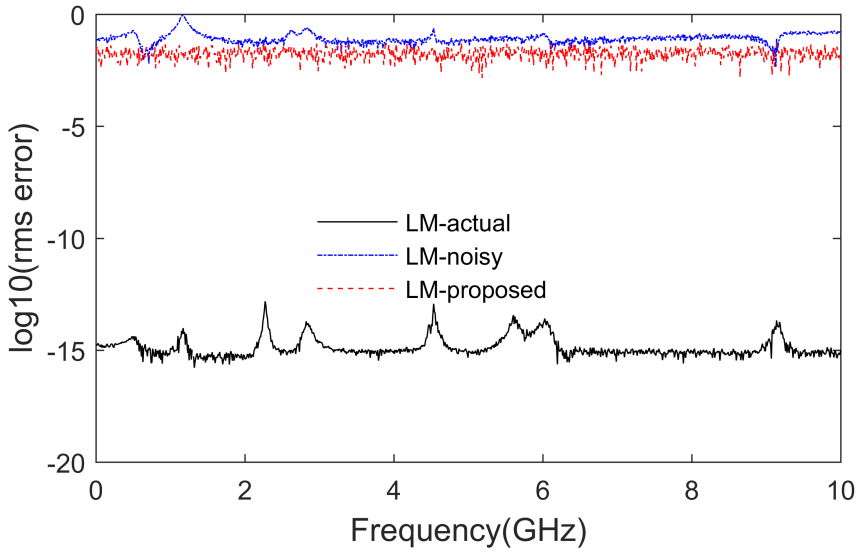

Figure 3.11: Log10(RMS error) vs. frequency plots for actual (noise-free) data approximation with LM (black), noisy data approximation with LM (blue) and noisy data approximation with LM-proposed (red) (Example 1)

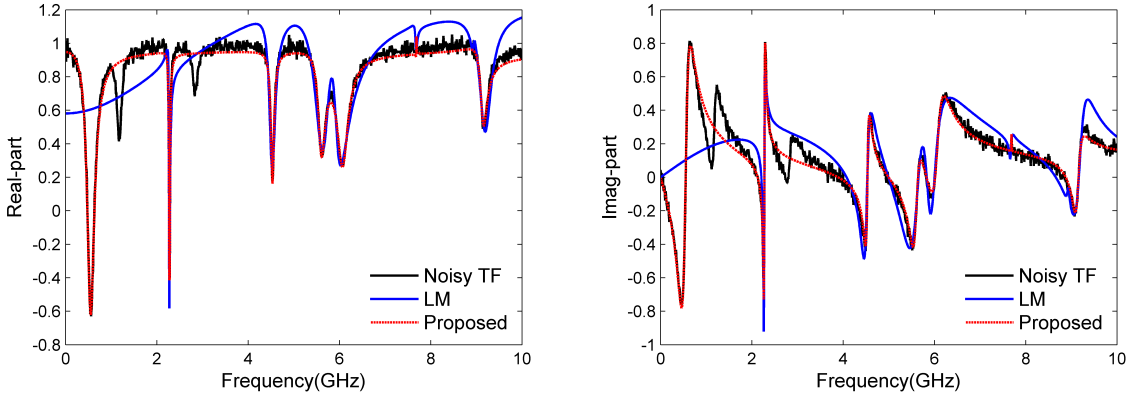

(a) (b)

Figure 3.12: Rational Approximation of the 16-dB SNR data using LM and LM-Proposed approximation. (a) Real part and (b) Imaginary part plots (Example 1).

Table 3.2: Calculated Poles Using LM and proposed method (Example 1) (SNR=18 dB)

LM		LM-Proposed	
Poles (GHz)	Error	Poles (GHz)	Error
-0.5440 ± 3.4970i	2.31%	-0.6123 ± 3.4556i	0.0285%
-57.9609 ± 75.6642i	1209.2%	-0.3922 ± 7.3793i	0.0534%
-0.0803 ± 14.2929i	0.085%	-0.0876 ± 14.3026i	0.0029%
-0.2563 ± 16.6408i	0.64%	-0.3973 ± 17.7809i	0.0764%
-0.3035 ± 28.3783i	0.29%	-0.2992 ± 28.4618i	0.0013%
-0.8762 ± 35.0419i	0.91%	-0.6387 ± 35.2633i	0.0199%
-0.7672 ± 37.7031i	0.94%	-1.0142 ± 37.9710i	0.0145%
-0.8999 ± 57.4897i	0.57%	-0.5720 ± 57.4780i	0.0058%

Table 3.3: Calculated Poles Using LM and proposed method (Example 1) (SNR=16 dB)

LM		LM-Proposed	
Poles (GHz)	Error	Poles (GHz)	Error
Missed pole	N/A	-0.6102 ± 3.4071i	1.3707%
Missed pole	N/A	Missed pole	N/A
-0.0727 ± 14.2661i	0.2752%	-0.0822 ±14.3026i	0.0406%
Missed pole	N/A	Missed pole	N/A
-0.4927 ± 28.3885i	0.7279%	-0.2675 ± 28.4702i	0.1147%
-1.4391 ± 35.4639i	2.3203%	-0.5848 ± 35.1600i	0.3473%
-1.0001 ± 37.1711i	2.0920%	-0.9123 ± 38.1052i	0.4541%
-1.0039 ± 57.6811i	0.8341%	-0.5498 ± 57.3972i	0.14%

Table 3.4: 100 simulations with different random noise (Example 1)

Example 1	order	LM average error	LM-proposed average error
18 dB	17	0.0813	0.0362
16 dB	19	0.0503	0.0297

Case 2:

Figure 3.12 shows the sample response of the TF with 16 dB SNR, TF from Loewner modeling and proposed LM method using 1000 sample points distributed evenly between 0-10 GHz.

Here order 17 was used to approximate the previous LM model. Table 3.3 shows that LM approximation missed three poles whereas our proposed iterative algorithm missed two poles. To verify the proposed algorithm, 100 simulations are performed with 18dB and 16dB SNRs with different random noise added to the TF. The average RMS error for LM and proposed iterative LM method are given in Table 3.4.

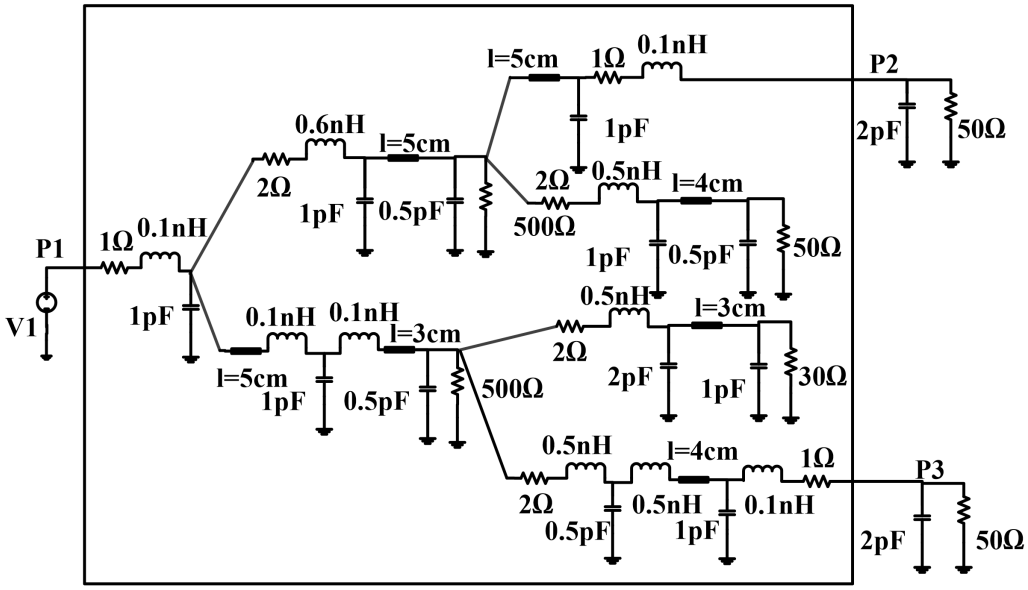

Figure 3.13: Transmission line network (Example 2)

3.4.2 Example 2

A transmission-line network is shown in Figure 3.13. The per-unit-length parameters of each line are $R = 8.26\Omega/m$, $L = 361nH/m$, $C = 140pF/m$, and $G = 0.0S/m$, and the length of the lines are listed in Figure 3.13. The Y-parameters of the three-port circuit described by the box of Figure 3.13 is calculated at 1000 frequency points distributed evenly between 0-10 GHz and treated as tabulated data. The data was generated using HSPICE. In this example, the added noise has an SNR of 25 dB and 20dB.

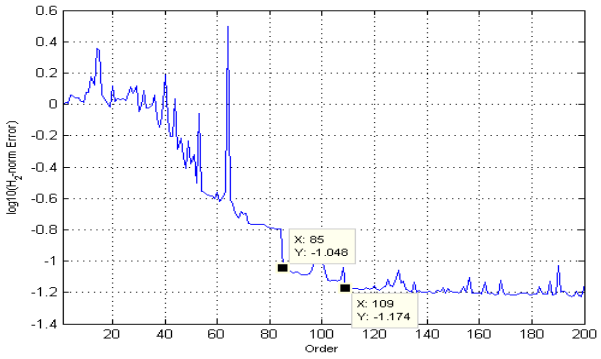

Figure 3.14: log10 (H_2 error) vs order for SNR=25dB (Example 2)

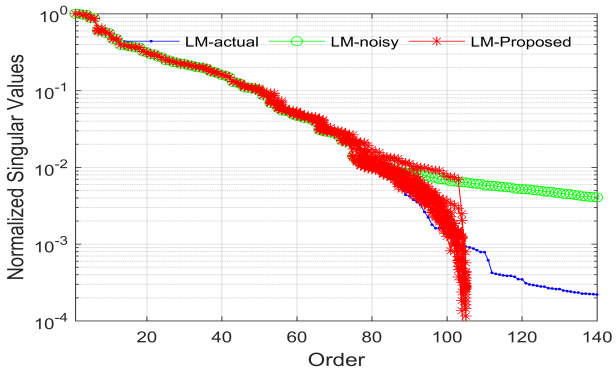

Figure 3.15: Normalized Singular Values (Example 2)

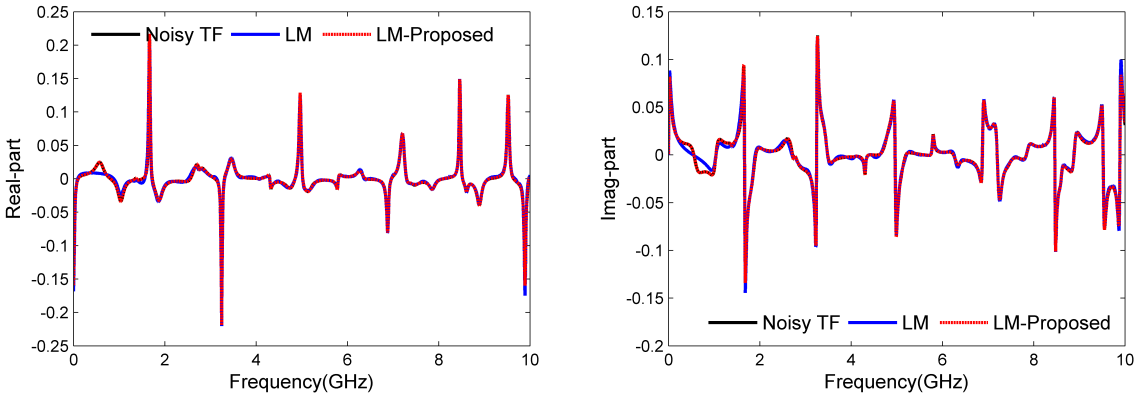

(a) (b)

Figure 3.16: Rational Approximation of Y(1,3) (Example 2)(SNR=25dB).

Case 1:

For SNR=25 dB, a range of order between 85 to 109 is found from Figure 3.14 showing LM approximated model log10(H_2 error) vs. order graph. For all these orders proposed algorithm

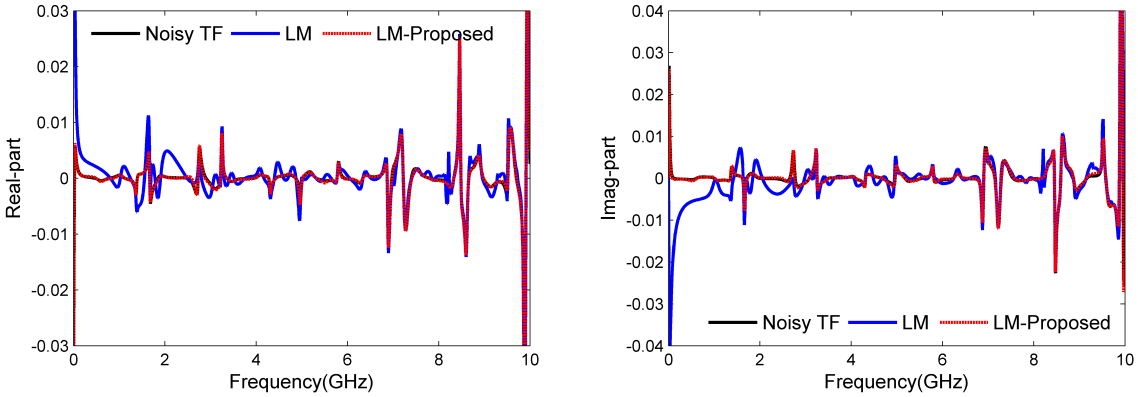

(a) (b)

Figure 3.17: Rational Approximation of Y(2,3) (Example 2) (SNR=25dB).

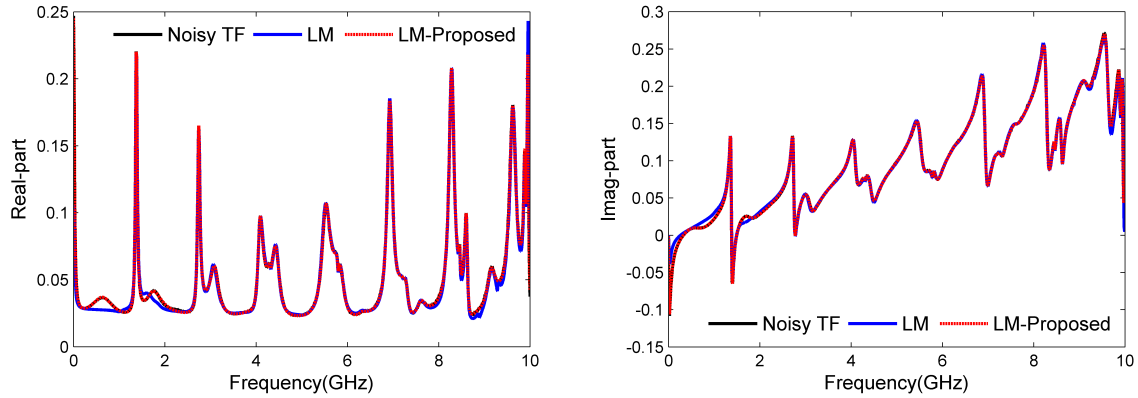

(a) (b)

Figure 3.18: Rational Approximation of Y(2,2) (Example 2) (SNR=25dB).

has been applied and order of the system is found 105. After choosing an order 105 normalized singular values are changed like Figure 3.15. Rational approximation of Y(1,3), Y(2,3) & Y(2,2) are shown is Figure 3.16, 3.17, 3.18 respectively. Figure 3.19 shows RMS error vs. iteration count for Y(1,3), Y(2,3) & Y(2,2). Figure 3.20 depicts H_2 error vs. iteration count for SNR=25dB for Example 2. H_2-norm error of the system is calculated as follows:

$$H_2\ error = \sqrt{\frac{\sum_{k=1}^{N_s} \|Y_{app}(s_k) - Y(s_k)\|_F^2}{\sum_{k=1}^{N_s} \|Y(s_k)\|_F^2}} \tag{3.23}$$

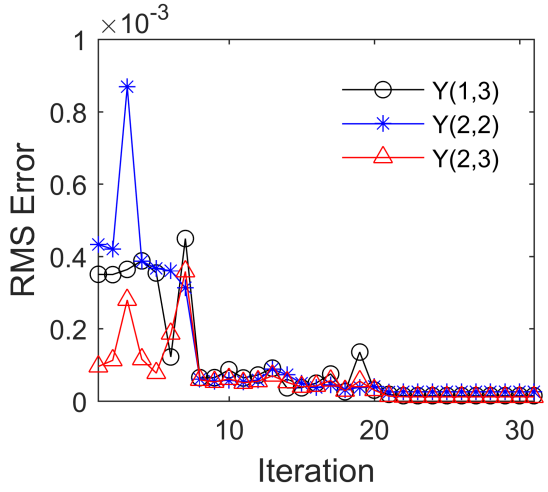

Figure 3.19: RMS error versus iteration count for SNR=25 dB (Example 2).

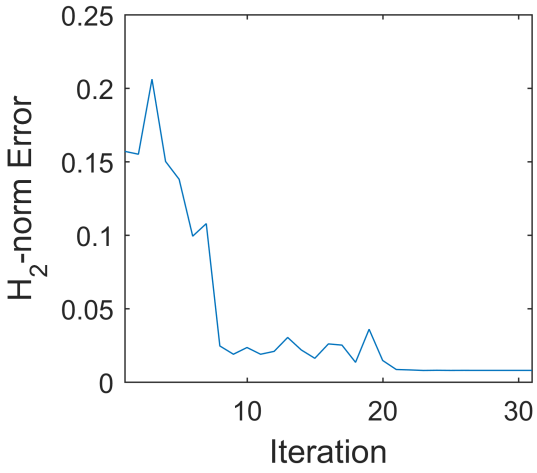

Figure 3.20: H_2-norm error versus iteration count for SNR=25 dB (Example 2)

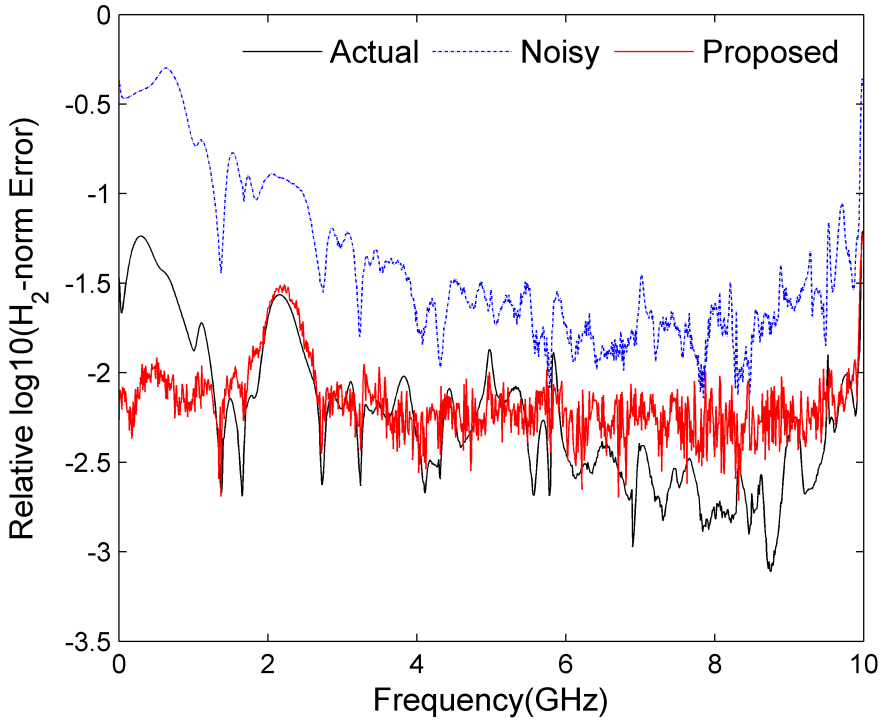

Figure 3.21: LM approximation of actual/noise-free data (black), LM approximation with noisy data (Blue) and proposed method approximation (Red) for order 105 (Example 2) (SNR=25dB)

Figure 3.21 shows comparison between LM approximation of actual/noise-free data, LM approximation with noisy data and proposed method with noisy data approximation for order 105

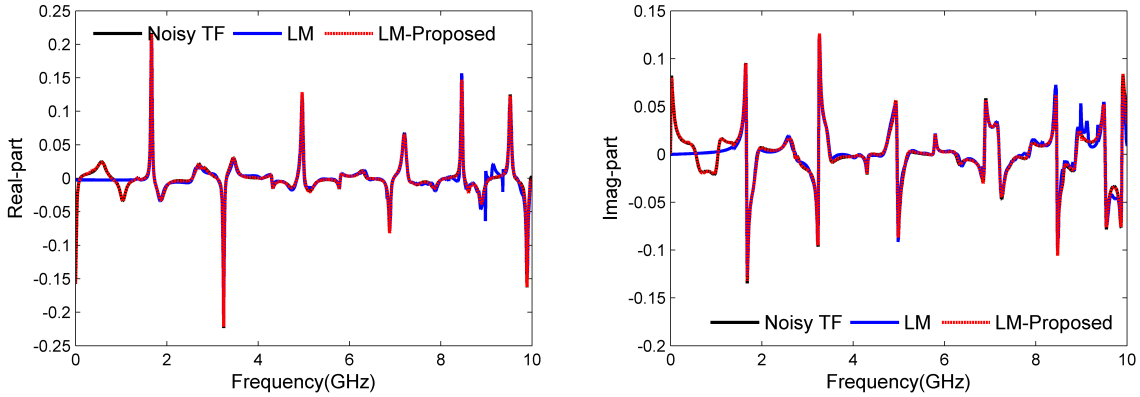

(a) (b)

Figure 3.22: Rational Approximation of Y(1,3) (Example 2) (SNR=20dB)

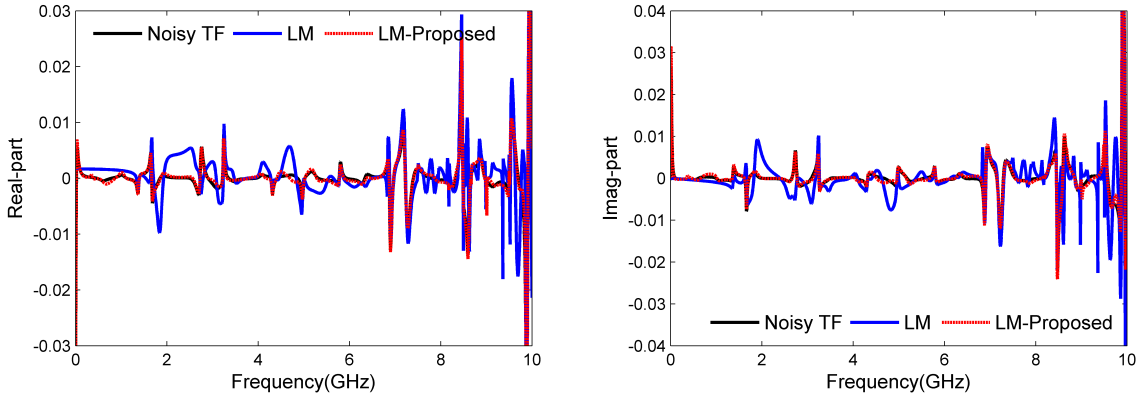

(a) (b)

Figure 3.23: Rational Approximation of Y(2, 3) (Example 2) (SNR=20dB).

using the following equation at each frequency point,

$$H_2\ error\ (s_k) = \sqrt{\frac{\|Y_{app}(s_k) - Y(s_k)\|_F^2}{\|Y(s_k)\|_F^2}} \tag{3.24}$$

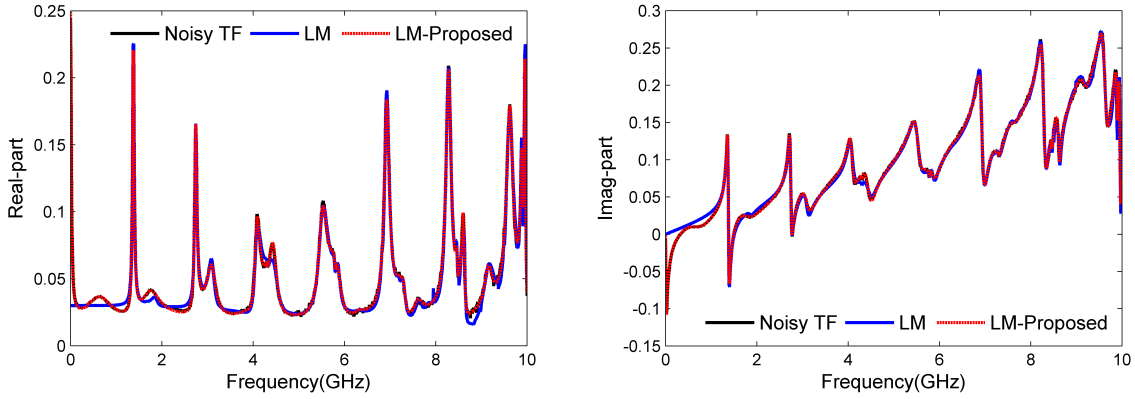

(a) (b)

Figure 3.24: Rational Approximation of Y(2, 2) (Example 2) (SNR=20dB).

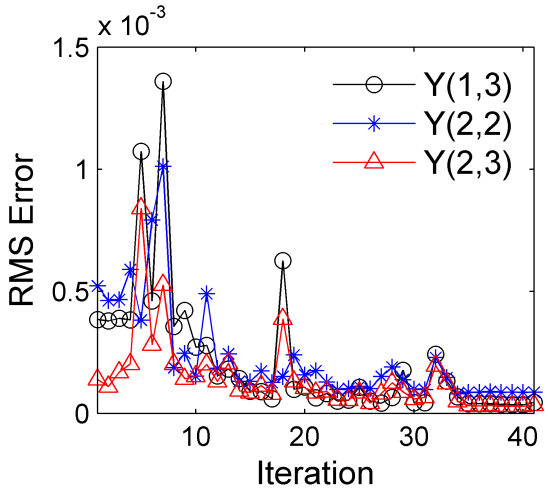

Figure 3.25: RMS error versus iteration count for SNR=20 dB (Example 2).

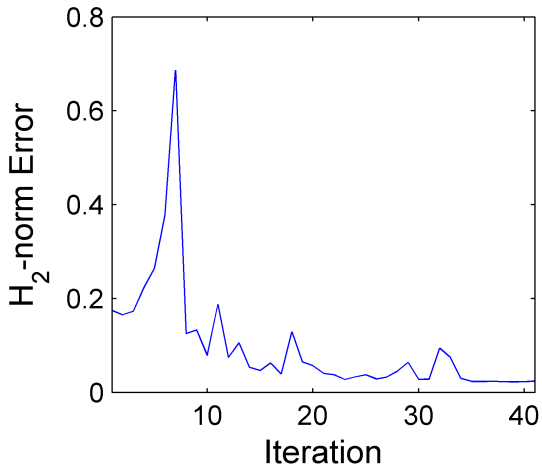

Figure 3.26: H_2-norm error versus iteration count for SNR=20 dB (Example 2)

Case 2:

For SNR=20 dB, order of the system is found 120. Figure 3.22, 3.23 and 3.24 show rational approximation of Y(1, 3), Y(2, 3) & Y(2, 2) respectively. Figure 3.25 shows RMS error vs. iteration count for Y(1, 3), Y(2, 3) & Y(2, 2). Figure 3.26 depicts H_2 error vs. iteration count for SNR=20dB for Example 2. Figure 3.27 shows comparison between LM approximation of actual (noise-free) data, LM approximation with noisy data and proposed method approximation with noisy data for order 120.

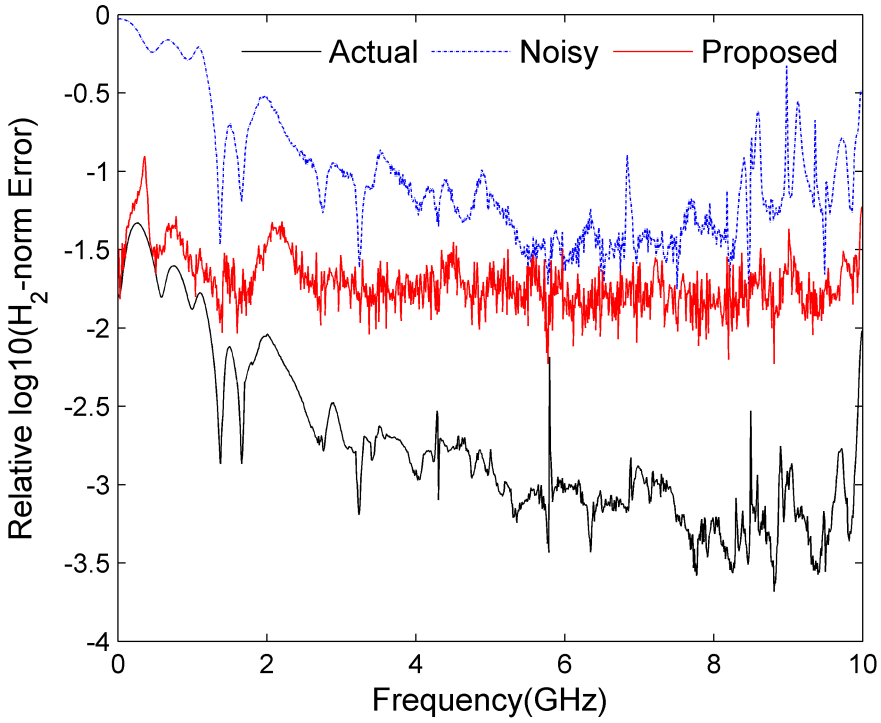

Figure 3.27: LM approximation of actual (noise-free) data (Black), LM approximation with noisy data (Blue) and proposed method approximation (Red) for order 120 (Example 2) (SNR= 20dB)

3.4.3 Example 3

This is an example of 18 port transmission line network depicted in Figure 3.28, containing nine coupled lines and nine noncoupled lines. Models for both coupled and noncoupled lines are shown in [2]. The parameter values for the coupled line are taken from [58]. The parameter values (per unit length) for noncoupled line are $R = 3.74\Omega/m$, $L = 283.7nH/m$, $C = 84.6pF/m$, and $G = 0.0S/m$. The lengths of the coupled and non-coupled lines are 0.1m and 0.05m, respectively. The network is characterized by its terminal responses (Y-parameters) as tabulated data over a bandwidth of $0 - 7$ GHz. The data was generated using HSPICE. For this example, SNR=30dB noise is added to data according to Equation (3.20).

Figure 3.29 shows normalized SVD vs. order for SNR=30dB for this 18-port system. From this figure we can see that order is from 250 to 450. Thus we plot LM approximated H_2 error vs. order graph in Figure 3.30 for this range of orders. Then from Figure 3.30, the range of order to

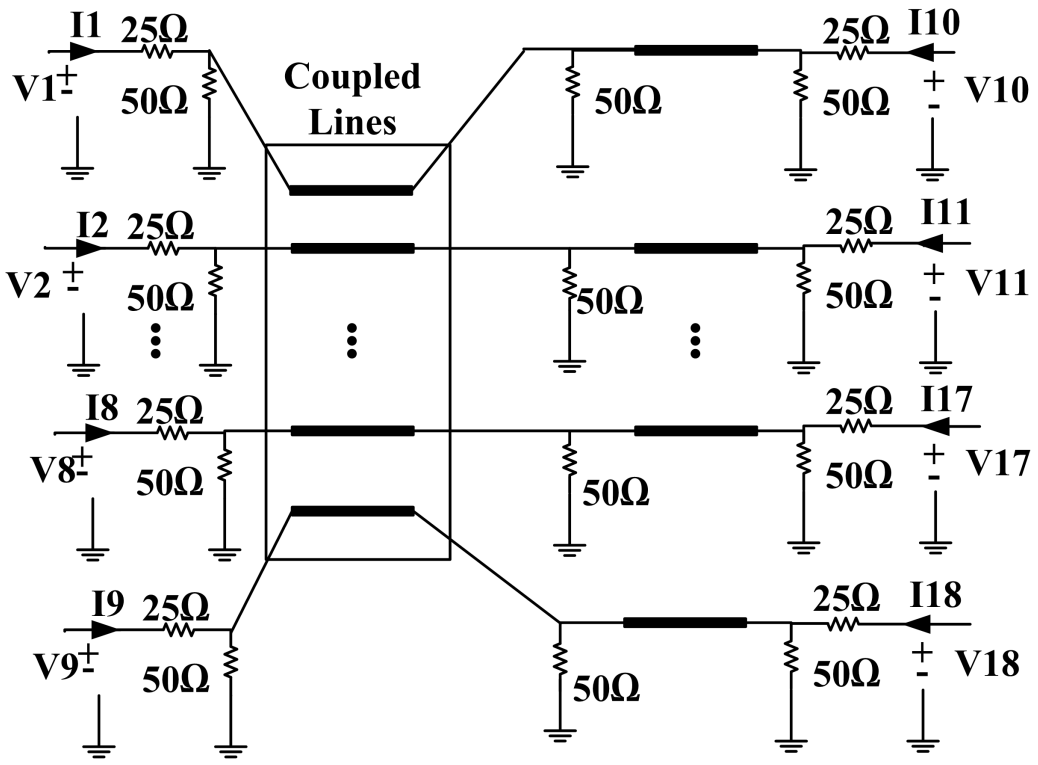

Figure 3.28: Circuit Diagram (Example 3)

apply our proposed algorithm is found from 370 to 391. The final order of the system is found to be 376 from Figure 3.31. Figure 3.32, 3.33 and 3.34 show the rational approximation of Y(1,18), Y(17,18) and Y(6,10) respectively. Comparison between LM approximation without noise data, LM approximation with noisy data and proposed method approximation for order 376 is shown in Figure 3.35.

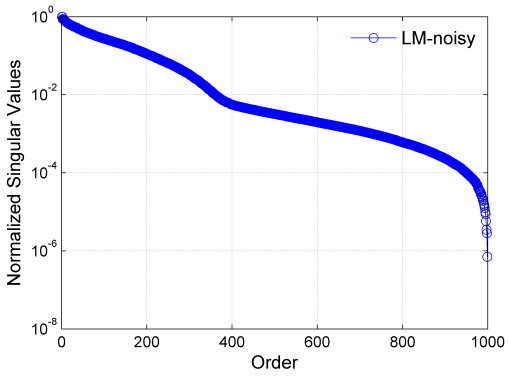

Figure 3.29: Normalized singular values vs. order for SNR=30dB (Example 3)

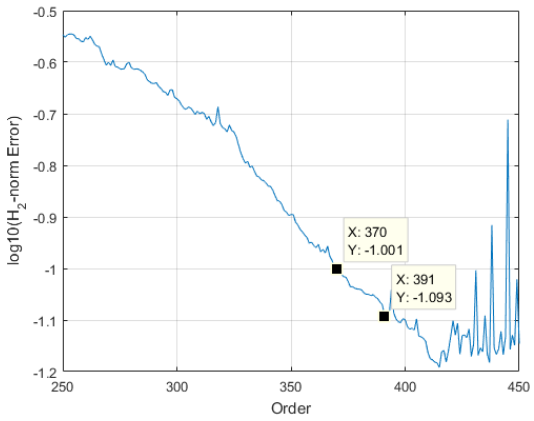

Figure 3.30: log10(H_2 error) vs. order for SNR=30 dB (Example 3)

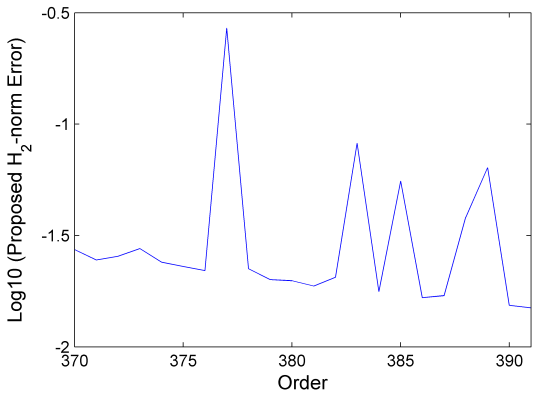

Figure 3.31: Proposed H_2 error vs. order for SNR=30 dB (Example 3)

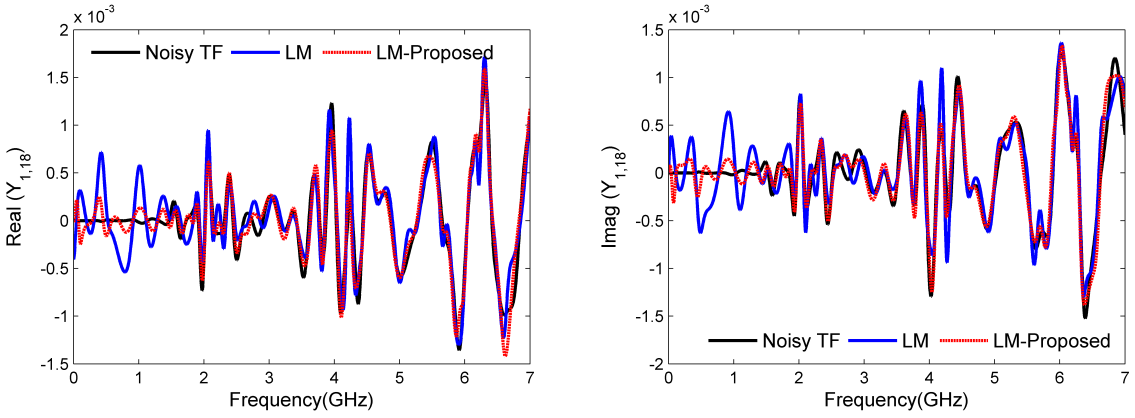

(a) (b)

Figure 3.32: Rational Approximation of Y(1,18) (Example 3).

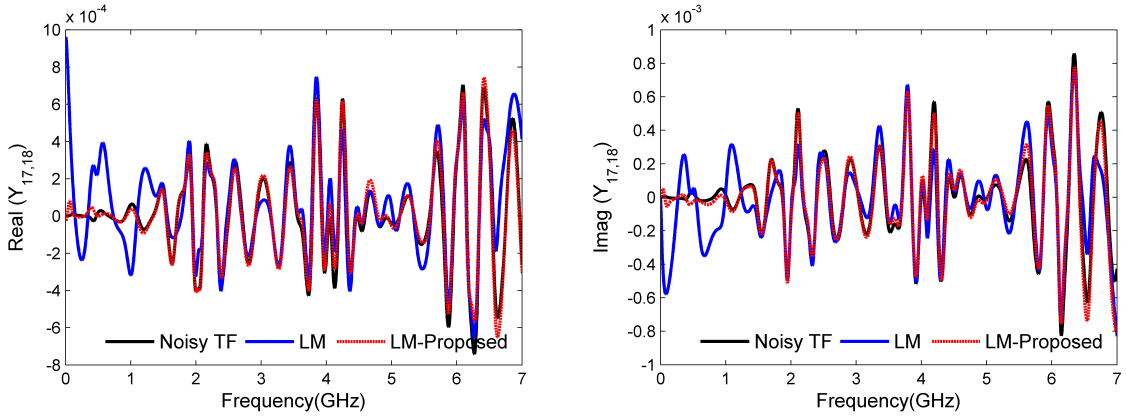

(a) (b)

Figure 3.33: Rational Approximation of Y(17,18) (Example 3).

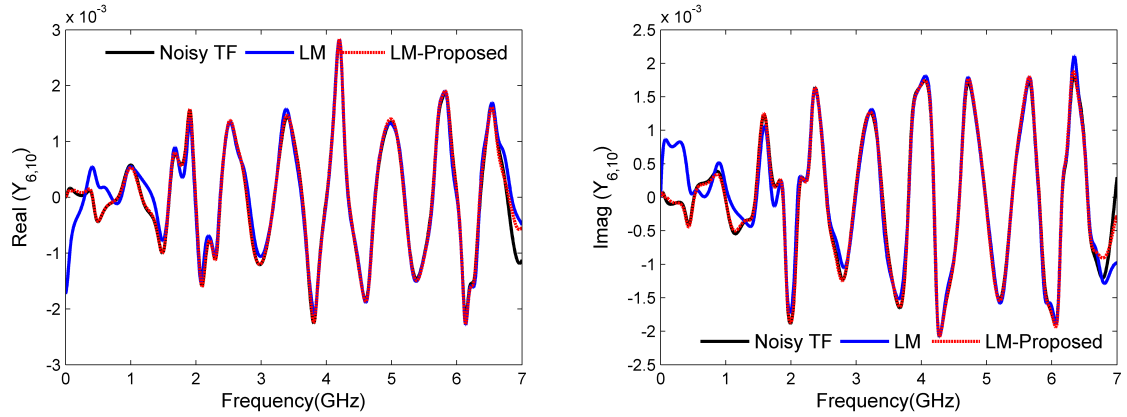

(a) (b)

Figure 3.34: Rational Approximation of Y(6,10) (Example 3).

3.4.4 Example 4

Figure 3.36 corresponds to a four-port network, which illustrates the far-end crosstalk between two differential pairs of StradaWhisper connectors provided by TE Connectivity, Harrisburg, PA. The network is characterized by real life measurements up to 20 GHz of the S-parameters using a vector network analyzer (VNA).

The order of the system was found to be 363. Figure 3.37, 3.38 and 3.39 represent the rational approximation of S(1, 3), S(2, 3) and S(2, 2). RMS error vs. iteration count for S(1,3), S(2,3) and S(2,2) is depicted in Figure 3.40 and H_2 error versus iteration count is in Figure 3.41. Relative H_2 norm error for noisy data LM approximation and noisy data proposed LM

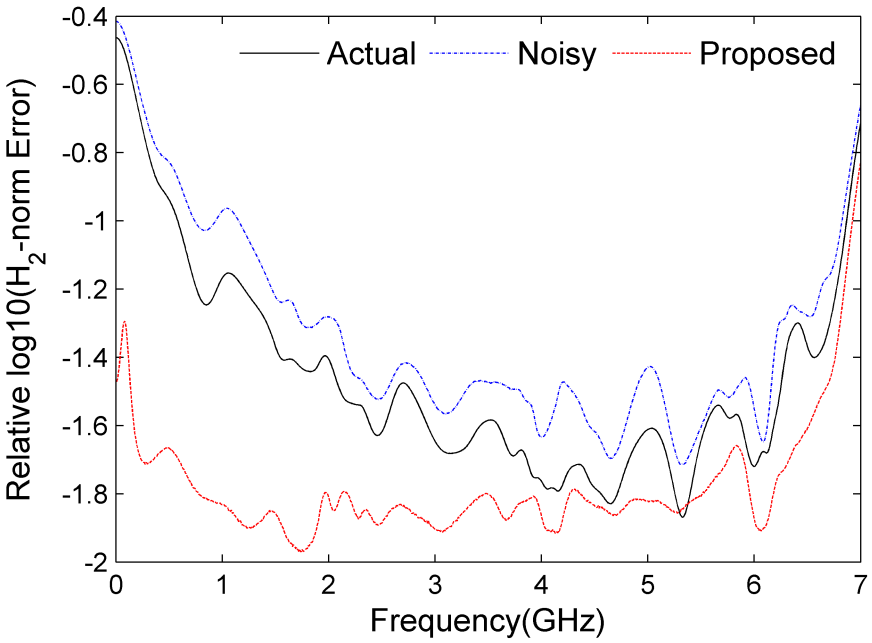

Figure 3.35: Relative Error of actual (noise-free) data LM approximation, noisy data LM approximation and proposed method LM approximation (Example 3)

approximation are presented in Figure 3.42.

3.5 Limitations of Proposed Method

As the noise in the data increases, the LM approximation becomes more inaccurate to identify the system. Therefore, too much noise present in the data will affect the approximation of the proposed method. For each iteration, we need to do SVD and Loewner Modeling of the data

Figure 3.36: Four-port network (Example 4).

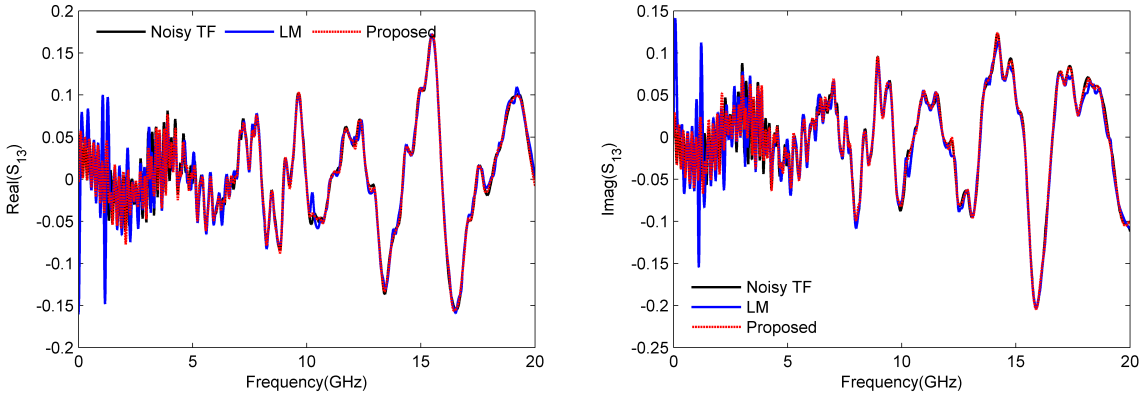

(a) (b)

Figure 3.37: Rational Approximation of S(1,3) (Example 4).

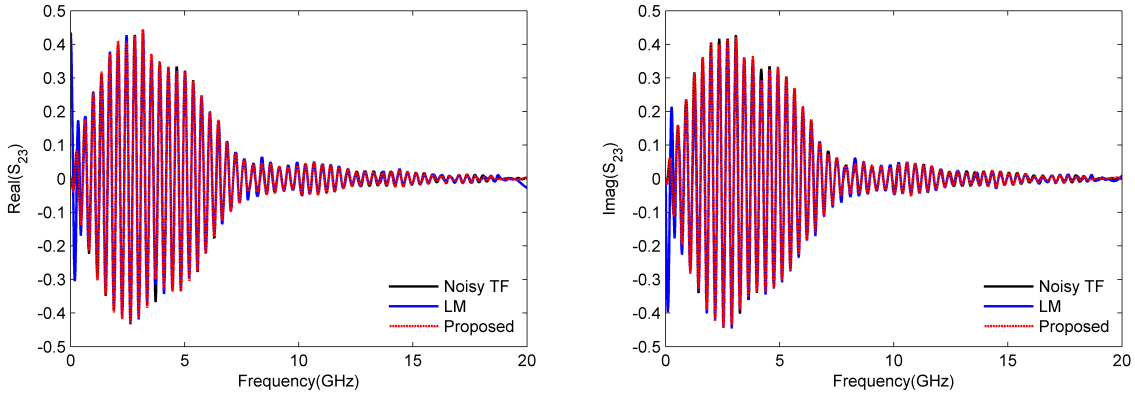

(a) (b)

Figure 3.38: Rational Approximation of S(2, 3) (Example 4).

which are CPU intensive task for large number of data. As a result, if the number of iteration increases our method will take longer time to approximate the data to identify the system.

3.6 Conclusion

In this chapter, an iterative Loewner modeling approach has been presented to increase the accuracy and efficiency of the Loewner matrix identification of a system for noisy frequency-domain responses. It is illustrated that by using the LM approximations from previous iteration to create the eigenvectors, biasing effect of the realization caused by the noisy data sample is

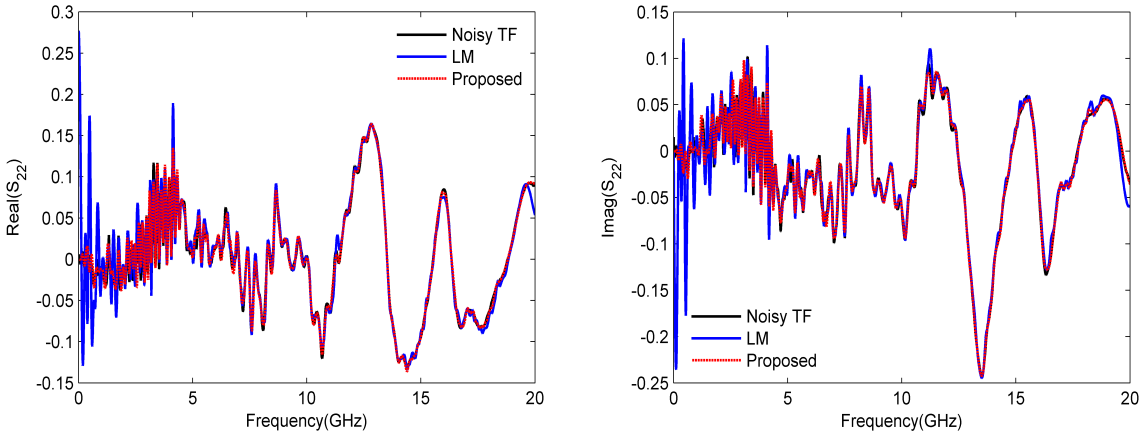

(a) (b)

Figure 3.39: Rational Approximation of S(2, 2) (Example 4).

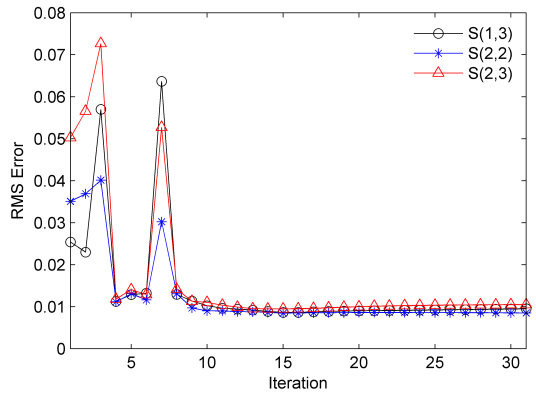

Figure 3.40: RMS error versus iteration count (Example 4).

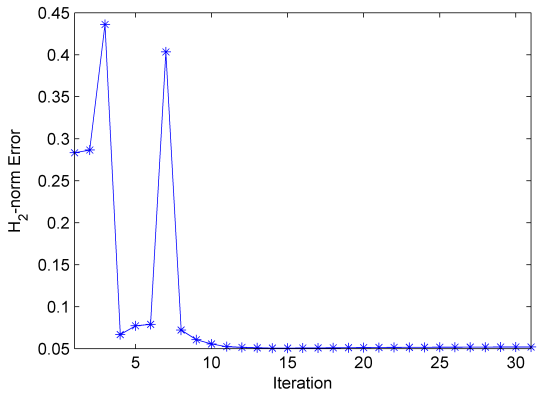

Figure 3.41: H_2-norm error versus iteration count (Example 4)

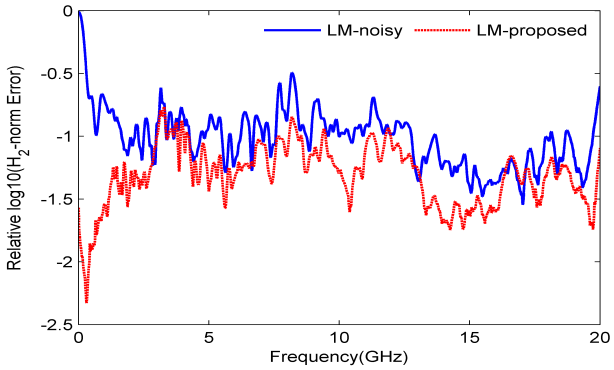

Figure 3.42: Relative Error of LM and Proposed Method (Example 4)

reduced. This improves the accuracy of the approximated TF.

Chapter 4

Fast Transient Analysis of Nonlinear Distributed Networks

4.1 Introduction

Interconnects are modeled to link them with nonlinear elements for transient analysis in circuit simulators. These modeling techniques give rise to many linear differential equations. At the termination of these interconnect networks there are nonlinear elements like drivers and receivers. These nonlinear components give rise to nonlinear differential equations. To convert differential equations into difference equations integration techniques are applied. Nonlinear difference equations are solved using Newton-Raphson iteration at each time step. Thus solving many nonlinear difference equations becomes a CPU intensive task for nonlinear circuit simulators [3]. By using Large Change Sensitivity [38, 39] method, these nonlinear parts can be separated from linear parts. During the time domain analysis only the matrices containing nonlinear terms need to be inverted. These matrices are very small matrices compared to matrices containing linear circuit equations. The cost of inverting a small matrix compared to a relatively very large matrix is really low. Thus use of this method will minimize the cost of CPU and make time-domain analysis faster.

4.2 Review of Large Change Sensitivity

Large Change Sensitivity (LCS) measures the variation in output due to change in linear elements like resistors, inductors, capacitors etc. in network equations [38, 39]. Let us consider a given network to be solved for specific nominal values of linear components. If some linear elements values are changed, LCS makes it possible without resolving the problem to obtain an exact solution. LCS method is summarized as follows:

Consider a network equation (n-sized) with linear elements assigned their nominal values,

$$T_0 X_0 = W \tag{4.1}$$

where, T_0 is the network matrix, X_0 is the network state vector, and W is the input excitation vector. The solution of (4.1) is:

$$X_0 = T_0^{-1} W \tag{4.2}$$

Let us suppose, m components of the network are subject to variations (can be from zero to infinity). The modified system can be described by,

$$TX = (T_0 + P\delta Q^t) = W \tag{4.3}$$

where, T and X are the new network matrix and new network state vector, $\delta = diag[\delta_i]$, $i = 1, \ldots, m$. Here P and Q are $n \times m$ matrices which contain 0 and ± 1 entries and indicate the location of the changed elements and described by,

$$\begin{aligned} P &= [p_1, p_2, ..., p_m] \\ Q &= [q_1, q_2, ..., q_m] \end{aligned} \tag{4.4}$$

In the direct approach, equation (4.3) is solved by factorization (LU decomposition) of the coefficient matrix T and followed by a series of forward/backward substitutions to find X. But,

when the number of the changed variables m is much smaller than the size of the system n, LCS approach offers a cheap computational cost compared to the direct approach.

$$T_0 X + P \underbrace{\delta \underbrace{Q^t X}_{\text{y}}}_{\text{z}} = W \tag{4.5}$$

$$T_0 X + P z = W \tag{4.6}$$

$$y = \delta^{-1} z \tag{4.7}$$

$$Q^t X = y \tag{4.8}$$

From (4.6),

$$X = T_0^{-1} W - T_0^{-1} P z \tag{4.9}$$

Substituting y from (4.7) and X from (4.9) into (4.8) and rearranging,

$$\delta^{-1} z + Q^t T_0^{-1} P z = Q^t T_0^{-1} W \tag{4.10}$$

$$z = (\delta^{-1} + Q^t T_0^{-1} P)^{-1} Q^t T_0^{-1} W = \delta (I + Q^t T_0^{-1} P \delta)^{-1} Q^t T_0^{-1} W \tag{4.11}$$

Substituting z into (4.9),

$$X = \underbrace{T_0^{-1} W}_{\text{Known}} - \underbrace{T_0^{-1} P \delta (I + Q^t T_0^{-1} P \delta)^{-1} Q^t \underbrace{T_0^{-1} W}_{\text{Known}}}_{\text{one forward/backward substitution}} \tag{4.12}$$

As a result, the new modified system can be solved by one forward/backward substitution and factorization of T matrix is not needed.

4.3 Large Change Sensitivity for Nonlinear Distributed Network Analysis

This section describes proposed LCS for nonlinear interconnect analysis.

4.3.1 Nonlinear Distributed Network Analysis

As described in Chapter 2, MNA equation of nonlinear distributed networks can be written by,

$$C_\psi \frac{dx(t)}{dt} + G_\psi(t) + F(x(t)) = b(t) \tag{4.13}$$

After using Trapezoidal rule, the difference equation becomes,

$$(\frac{C_\psi}{\Delta t} + \frac{G_\psi}{2})x_{t+1} + \frac{F(x_{t+1})}{2} - (\frac{C_\psi}{\Delta t} - \frac{G_\psi}{2})x_t + \frac{F(x_t)}{2} = \frac{b_t + b_{t+1}}{2} \tag{4.14}$$

After applying Newton-Raphson method the problem becomes solving the following function,

$$f^k_{t+1} = (\frac{C_\psi}{\Delta t} + \frac{G_\psi}{2})x_{t+1} + \frac{F(x_{t+1})}{2} - (\frac{C_\psi}{\Delta t} - \frac{G_\psi}{2})x_t + \frac{F(x_t)}{2} - \frac{b_t + b_{t+1}}{2} = 0 \tag{4.15}$$

x_{t+1} is solved at each iteration by applying

$$x^{k+1}_{t+1} = x^k_{t+1} + \Delta x^k_{t+1} \tag{4.16}$$

$$\Delta x^k_{t+1} = -((\frac{C_\psi}{\Delta t} + \frac{G_\psi}{2}) + \frac{1}{2}\frac{dF(x^k_{t+1})}{dx_{t+1}})^{-1} f^k_{t+1} \tag{4.17}$$

Here $(\frac{C_\psi}{\Delta t}+\frac{G_\psi}{2})+\frac{1}{2}\frac{dF(x^k_{t+1})}{dx_{t+1}}$ is an $n\times n$ Jacobian matrix. This matrix is usually very large matrix. To solve equation (4.17) at each step of Newton-Raphson iteration cost one LU decomposition and one forward/backward substitution making time domain analysis a CPU intensive task.

In the Jacobian matrix, $(\frac{C_\psi}{\Delta t} + \frac{G_\psi}{2})$ part comes from linear components and step size Δt is con-

stant. As a result, this part remains unchanged whereas $\frac{1}{2}\frac{dF(x_{t+1}^k)}{dx_{t+1}}$ part comes from nonlinear elements and changes at each step of iteration. As the number of nonlinear elements are very few compared to linear elements, $\frac{1}{2}\frac{dF(x_{t+1}^k)}{dx_{t+1}}$ matrix is very small compared to large linear matrix $(\frac{C_\psi}{\Delta t} + \frac{G_\psi}{2})$. Equation (4.17) can be solved using Large Change Sensitivity approach where a small nonlinear element matrix needs to be inverted at each step of Newton iteration. Cost of inverting a small matrix is much less than inverting a very large Jacobian matrix. Thus this method makes time domain analysis faster.

4.3.2 Application of LCS for Nonlinear Distributed Network Analysis

The unchanged network equation is given by,

$$\begin{aligned}(\frac{C_\psi}{\Delta t} + \frac{G_\psi}{2})x_{t+1}^k &= -f_{t+1}^k \\ \Rightarrow x_{t+1}^k &= -(\frac{C_\psi}{\Delta t} + \frac{G_\psi}{2})^{-1} f_{t+1}^k\end{aligned} \tag{4.18}$$

The equation describing the modified system with nonlinear parts is given by,

$$((\frac{C_\psi}{\Delta t} + \frac{G_\psi}{2}) + \frac{1}{2}\frac{dF(x_{t+1}^k)}{dx_{t+1}})\Delta x_{t+1}^k = -f_{t+1}^k \tag{4.19}$$

In conventional approach Δx_{t+1}^k is solved by one LU decomposition and one forward/backward substitution of Jacobian matrix $(\frac{C_\psi}{\Delta t} + \frac{G_\psi}{2}) + \frac{1}{2}\frac{dF(x_{t+1}^k)}{dx_{t+1}}$ at each Newton iteration.
The variation in x_{t+1}^k due to $\frac{1}{2}\frac{dF(x_{t+1}^k)}{dx_{t+1}}$ is calculated using LCS approach. To apply Large Change Sensitivity, $\frac{1}{2}\frac{dF(x_{t+1}^k)}{dx_{t+1}}$ is parted into three matrices like,

$$\frac{1}{2}\frac{dF(x_{t+1}^k)}{dx_{t+1}} = P\delta Q^t$$

Here P and Q are $n \times m$ incident matrices which contain 0 and ± 1 entries and are associated with the nonlinear devices. Here n is the size of the system and m depends on number of

currents passing through nonlinear devices.

$$\begin{aligned} P &= [p_1, p_2, ..., p_m] \\ Q &= [q_1, q_2, ..., q_m] \end{aligned} \tag{4.20}$$

and δ is a diagonal $m \times m$ matrix. δ is the derivative of the currents of nonlinear elements with respect to node voltages.

$$\delta = diag[\delta_i] = \frac{1}{2}\frac{dF(x^k_{t+1})}{dx_{t+1}} \tag{4.21}$$

LCS technique reduces substantial computational cost when number of currents passing through nonlinear devices m, is much smaller than the size of the system n. By applying LCS, equation (4.19) becomes,

$$(\frac{C_\psi}{\Delta t} + \frac{G_\psi}{2})\Delta x^k_{t+1} + P\,\underbrace{\delta\,\underbrace{Q^t \Delta x^k_{t+1}}_{\text{y}}}_{\text{z}} = -f^k_{t+1} \tag{4.22}$$

$$(\frac{C_\psi}{\Delta t} + \frac{G_\psi}{2})\Delta x^k_{t+1} + Pz = -f^k_{t+1} \tag{4.23}$$

$$y = \delta^{-1} z \tag{4.24}$$

$$Q^t \Delta x^k_{t+1} = y \tag{4.25}$$

From (4.23),

$$\Delta x^k_{t+1} = -(\frac{C_\psi}{\Delta t} + \frac{G_\psi}{2})^{-1} f^k_{t+1} - (\frac{C_\psi}{\Delta t} + \frac{G_\psi}{2})^{-1} Pz \tag{4.26}$$

Substituting y from (4.24) and Δx^k_{t+1} from (4.26) into (4.25) and rearranging,

$$\delta^{-1} z + Q^t(\frac{C_\psi}{\Delta t} + \frac{G_\psi}{2})^{-1} Pz = -Q^t(\frac{C_\psi}{\Delta t} + \frac{G_\psi}{2})^{-1} f^k_{t+1} \tag{4.27}$$

$$\begin{aligned} z &= -(\delta^{-1} + Q^t(\frac{C_\psi}{\Delta t} + \frac{G_\psi}{2})^{-1} P)^{-1} Q^t(\frac{C_\psi}{\Delta t} + \frac{G_\psi}{2})^{-1} f^k_{t+1} \\ &= -\delta(I + Q^t(\frac{C_\psi}{\Delta t} + \frac{G_\psi}{2})^{-1} P\delta)^{-1} Q^t(\frac{C_\psi}{\Delta t} + \frac{G_\psi}{2})^{-1} f^k_{t+1} \end{aligned} \tag{4.28}$$

Substituting z from (4.28) into (4.26) we can get,

$$\Delta x_{t+1}^{k} = -(\frac{C_\psi}{\Delta t}+\frac{G_\psi}{2})^{-1} f_{t+1}^{k} + (\frac{C_\psi}{\Delta t}+\frac{G_\psi}{2})^{-1} P\delta (I + Q^t (\frac{C_\psi}{\Delta t}+\frac{G_\psi}{2})^{-1} P\delta)^{-1} Q^t (\frac{C_\psi}{\Delta t}+\frac{G_\psi}{2})^{-1} f_{t+1}^{k} \quad (4.29)$$

Thus Δx_{t+1}^{k} can be solved using equation (4.29) by using LCS approach. An illustrative example has been presented in the following section.

4.3.3 Illustrative Example

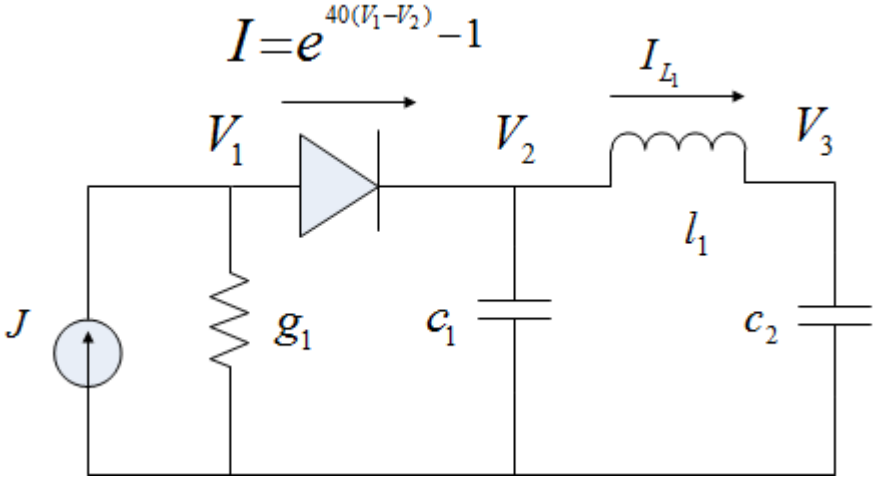

Figure 4.1: Illustrative LCS example

To describe the process consider the nonlinear circuit shown in Figure 4.1. The individuals presented in equation (4.13) with respect to the given nonlinear circuit network can be obtained by,

$$G_\psi = \begin{bmatrix} g_1 & 0 & 0 & 0 \\ 0 & 0 & 0 & 1 \\ 0 & 0 & 0 & -1 \\ 0 & 1 & -1 & 0 \end{bmatrix} \quad C_\psi = \begin{bmatrix} 0 & 0 & 0 & 0 \\ 0 & c_1 & 0 & 0 \\ 0 & 0 & c_2 & 0 \\ 0 & 0 & 0 & -l_1 \end{bmatrix}$$

$$F = \begin{bmatrix} e^{40(V_1-V_2)} - 1 \\ -e^{40(V_1-V_2)} + 1 \\ 0 \\ 0 \end{bmatrix} \quad x = \begin{bmatrix} V_1 \\ V_2 \\ V_3 \\ I_{L_1} \end{bmatrix} \quad b = \begin{bmatrix} J \\ 0 \\ 0 \\ 0 \end{bmatrix}$$

$$\frac{1}{2}\frac{dF}{dx} = \frac{1}{2}\begin{bmatrix} 40e^{40(V_1-V_2)} & -40e^{40(V_1-V_2)} & 0 & 0 \\ -40e^{40(V_1-V_2)} & 40e^{40(V_1-V_2)} & 0 & 0 \\ 0 & 0 & 0 & 0 \\ 0 & 0 & 0 & 0 \end{bmatrix} = P\delta Q^t$$

Now to apply Large Change Sensitivity approach, P, δ and Q matrices for this example are described as,

$$P = \begin{bmatrix} 1 \\ -1 \\ 0 \\ 0 \end{bmatrix} \quad \delta = \frac{1}{2}\left[40e^{40(V_1-V_2)}\right] \quad Q^t = \begin{bmatrix} 1 & -1 & 0 & 0 \end{bmatrix}$$

Using conventional approach Δx_{t+1}^k can be solved by,

$$\Delta x_{t+1}^k = - \underbrace{((\frac{C_\psi}{\Delta t} + \frac{G_\psi}{2}) + \frac{1}{2}\frac{dF(x_{t+1}^k)}{dx_{t+1}})^{-1} f_{t+1}^k}_{\text{one LU decomposition and one forward/backward substitution}} \tag{4.30}$$

Using LCS Δx_{t+1}^k can be calculated by,

$$\Delta x_{t+1}^k = - \underbrace{(\frac{C_\psi}{\Delta t} + \frac{G_\psi}{2})^{-1} f_{t+1}^k}_{\text{first forward/backward substitution}}$$
$$+ \underbrace{(\frac{C_\psi}{\Delta t} + \frac{G_\psi}{2})^{-1} P\delta \underbrace{(I + Q^t(\frac{C_\psi}{\Delta t} + \frac{G_\psi}{2})^{-1} P\delta)^{-1}}_{\text{an } 1\times 1 \text{ matrix inversion}} Q^t \quad \underbrace{(\frac{C_\psi}{\Delta t} + \frac{G_\psi}{2})^{-1} f_{t+1}^k}_{\text{first forward/backward substitution}}}_{\text{second forward/backward substitution}} \tag{4.31}$$

One LU decomposition costs equals three forward/backward substitutions. Using conventional approach Δx_{t+1}^k is solved by one LU decomposition and one forward/backward substitution at each Newton iteration. As $(\frac{C_\psi}{\Delta t} + \frac{G_\psi}{2})$ is fixed during the simulation, using LCS approach LU decomposition of $(\frac{C_\psi}{\Delta t} + \frac{G_\psi}{2})$ is done only once in the entire simulation. This LU decomposition has been reused to determine Δx_{t+1}^k with two forward/backward substitution and a small matrix inversion at each Newton iteration. This makes time domain analysis faster than the conventional approach.

4.3.4 Cost of Applying LCS for Nonlinear Circuit Simulation

Using the proposed approach the total simulation cost becomes $(2N_R C_{FB} + C_{LU})$ whereas the total cost for conventional approach is $(N_R(C_{FB} + C_{LU}))$, where N_R is the total number of Newton-Raphson iteration, C_{LU} is cost of LU decomposition of $(\frac{C_\psi}{\Delta t} + \frac{G_\psi}{2})$ and C_{FB} is the cost of forward/backward substitutions for solving $(\frac{C_\psi}{\Delta t} + \frac{G_\psi}{2})^{-1} f_{t+1}^k$ and $(\frac{C_\psi}{\Delta t} + \frac{G_\psi}{2})^{-1} P\delta(I + Q^t(\frac{C_\psi}{\Delta t} + \frac{G_\psi}{2})^{-1} P\delta)^{-1} Q^t(\frac{C_\psi}{\Delta t} + \frac{G_\psi}{2})^{-1} f_{t+1}^k$.

4.4 Numerical Examples

Four numerical examples are given here. Two types of modeling approaches have been used here. Interconnects of the first three examples are modeled using distributed lumped modeling. Interconnect network of the last example has been modeled from frequency domain data using Loewner matrix method approach. All timing results are executed in MATLAB 2014b on 64-bit operating system with Intel(R) Core(TM) i5660 CPU at 3.33 GHz and 4 GB RAM.

4.4.1 Example 1

The circuit considered in this example is shown in Figure 4.2. It contains three lossy TLs numbered by sub-circuits $1-3$. The lengths of the TLs in sub-circuits $1-3$ are 0.04, 0.1, and

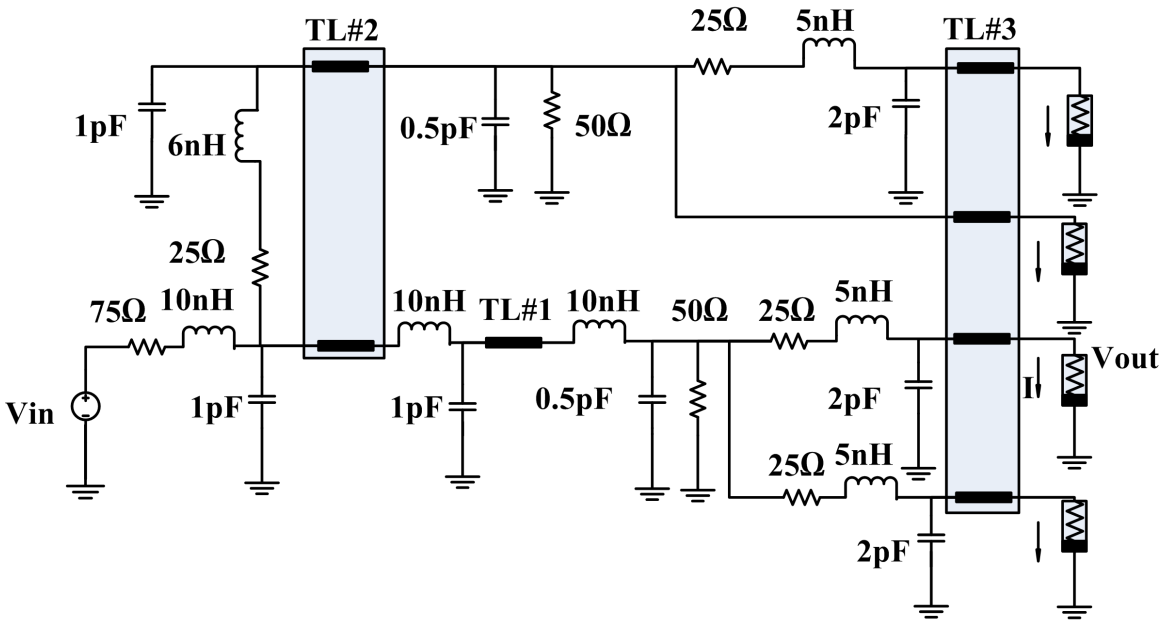

Figure 4.2: Circuit containing three lossy TLs (Example 1)

0.06 m, respectively. The electrical parameters of TL#1 are $L_1 = 600$ nH/m, $C_1 = 1$ nF/m, $R_1 = 1\Omega$/m, and $G_1 = 5$ mS/m. The parameters of TL#2 are

$$L_2 = \begin{bmatrix} 600 & 50 \\ 50 & 600 \end{bmatrix} \text{nH/m}$$

$$C_2 = \begin{bmatrix} 1.2 & -0.11 \\ -0.11 & 1.2 \end{bmatrix} \text{nF/m}$$

$$R_2 = \begin{bmatrix} 2.25 & 0 \\ 0 & 2.25 \end{bmatrix} \Omega\text{/m}$$

$$G_2 = \begin{bmatrix} 7.5 & 0 \\ 0 & 7.5 \end{bmatrix} \text{mS/m}$$

The parameters of TL#3 are

Table 4.1: Simulation Results using Conventinal matrix inversion and Proposed LCS method

	Modeling	Variable size	Conventional (sec)	Proposed (sec)	Improvement (times)
Example 1	Lumped	981	26.040	10.956	2.37
Example 2	Lumped	1513	61.057	27.758	2.20
Example 3	Lumped	1809	21.626	7.809	2.76
Example 4	Loewner	481	166.831	51.164	3.26

$$L_3 = \begin{bmatrix} 1 & 0.11 & 0.03 & 0 \\ 0.11 & 1 & 0.11 & 0.03 \\ 0.03 & 0.11 & 1 & 0.11 \\ 0 & 0.03 & 0.11 & 1 \end{bmatrix} \mu\text{H/m}$$

$$C_3 = \begin{bmatrix} 1.5 & -0.17 & -0.03 & 0 \\ -0.07 & 1.5 & -0.07 & -0.03 \\ -0.03 & -0.07 & 1.5 & -0.07 \\ 0 & -0.03 & -0.07 & 1.5 \end{bmatrix} \text{nF/m}$$

$$R_3 = \begin{bmatrix} 3.5 & 0 & 0 & 0 \\ 0 & 3.5 & 0 & 0 \\ 0 & 0 & 3.5 & 0 \\ 0 & 0 & 0 & 3.5 \end{bmatrix} \Omega\text{/m}$$

$$G_3 = \begin{bmatrix} 10 & 1 & 0.1 & 0 \\ 1 & 10 & 1 & 0.1 \\ 0.1 & 1 & 10 & 1 \\ 0 & 0.1 & 1 & 10 \end{bmatrix} \text{mS/m}$$

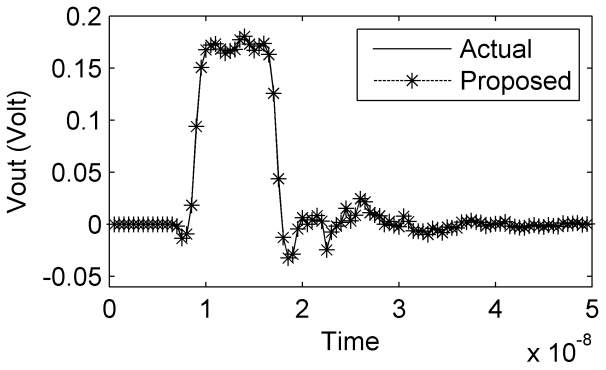

Figure 4.3: Transient response of the circuit shown in Figure 4.1 at node V_{out}

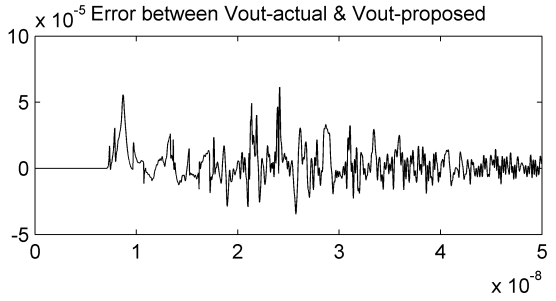

Figure 4.4: Error at node V_{out}

The applied voltage is a trapezoidal pulse with a rise and fall time of 1 ns, a pulsewidth of 7 ns, and a magnitude of 2 V. Lumped sections for TLs in sub-circuits $1-3$ are 20, 54, and 48 respectively. All nonlinear resistors follow the $I = V^3$ relation. The voltage response at node V_{out} is shown in Figure 4.3. Error at node V_{out} between two methods is given in Figure 4.4.

4.4.2 Example 2

In this example, an interconnect system depicted in Figure 4.5 with several multiconductor transmission lines is considered. The lengths of the TLs are 0.05 cm. The applied voltage is a trapezoidal pulse with a rise and fall time of 0.1 ns, a pulsewidth of 10 ns, and a magnitude of 3 V. For lumped modeling 20 sections are used. The transient response at node M1 using conventional matrix inversion and proposed LCS method is shown in Figure 4.6. The p.u.l. parameters of the coupled lines are

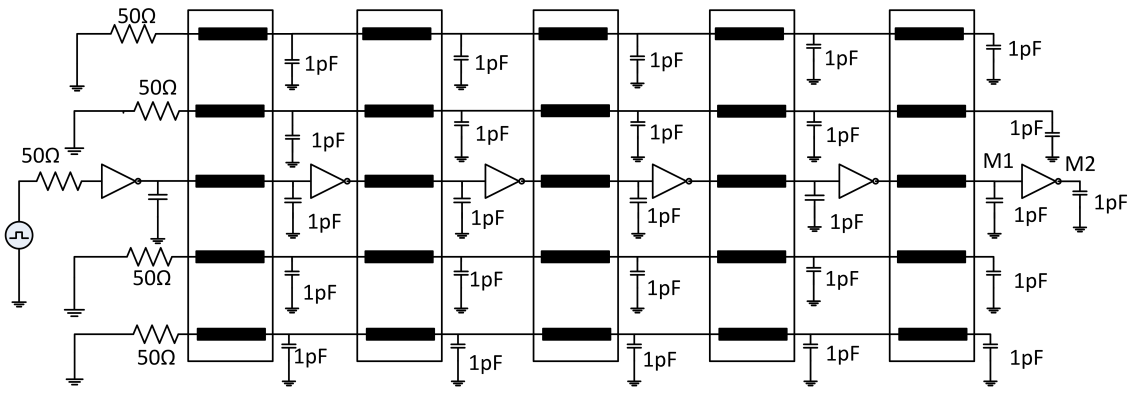

Figure 4.5: Circuit of (Example 2)

$$C_5 = \begin{bmatrix} 1.32 & -0.75 & -0.0363 & -0.0154 & -0.0147 \\ -0.75 & 1.80 & -0.74 & -0.0285 & -0.0154 \\ -0.0363 & -0.74 & 1.80 & -0.73 & -0.0154 \\ -0.0154 & -0.0285 & -0.73 & 1.78 & -0.75 \\ -0.0147 & -0.0154 & -0.0154 & -0.75 & 1.32 \end{bmatrix} \text{pF/cm}$$

$$L_5 = \begin{bmatrix} 3.89 & 2.19 & 1.33 & 0.86 & 0.60 \\ 2.19 & 3.71 & 2.10 & 1.29 & 0.86 \\ 1.33 & 2.10 & 3.67 & 2.10 & 1.33 \\ 0.86 & 1.29 & 2.10 & 3.71 & 2.19 \\ 0.60 & 0.86 & 1.33 & 2.19 & 3.89 \end{bmatrix} \mu\text{H/cm}$$

$$R_5 = \begin{bmatrix} 3.5 & 0 & 0 & 0 \\ 0 & 3.5 & 0 & 0 \\ 0 & 0 & 3.5 & 0 \\ 0 & 0 & 0 & 3.5 \end{bmatrix} \Omega\text{/cm}$$

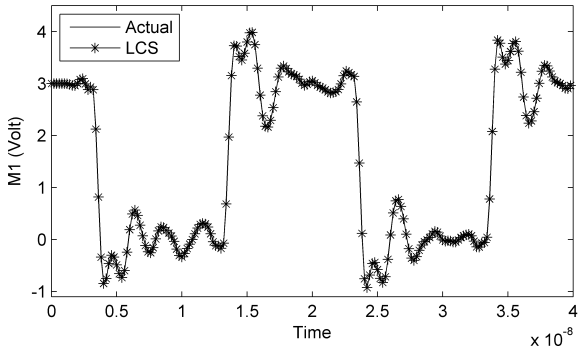

Figure 4.6: Transient Analysis at node M1 of Example 2

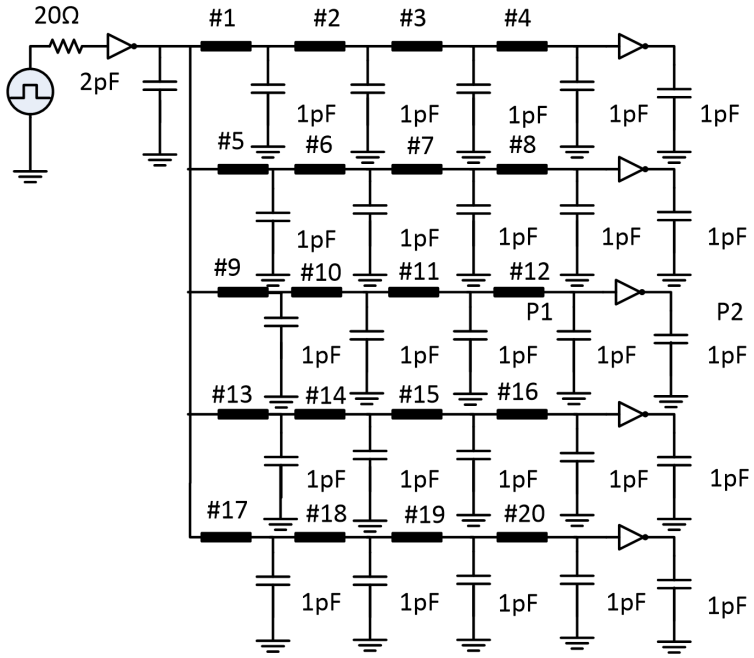

Figure 4.7: Circuit of (Example 3)

4.4.3 Example 3

The third example in Figure 4.7 has twenty interconnect lines with six non-linear inverters. The length of the TLs #1, 2, 3, 10, 11, 12 are 0.1 cm, #4, 5, 13, 14, 15, 18, 19, 20 are 0.2cm, and #6, 7, 8, 9, 16, 17 are 0.3 cm. The per unit length parameters of the interconnect lines are $L = 11.6\ \mu$H/cm, $C = 3.22$ pF/cm, $R = 338\ \Omega$/cm. Here the applied voltage is a trapezoidal pulse with a rise and fall time of 1.2223 ns, a pulsewidth of 48.78 ns, and a magnitude of 3 V. Here 30 lumped sections are used for all TLs. The transient response at node P1 is presented

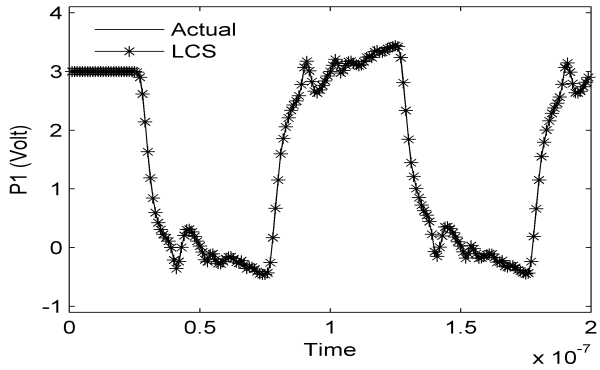

Figure 4.8: Transient Analysis at node P1 of Example 3

in Figure 4.8.

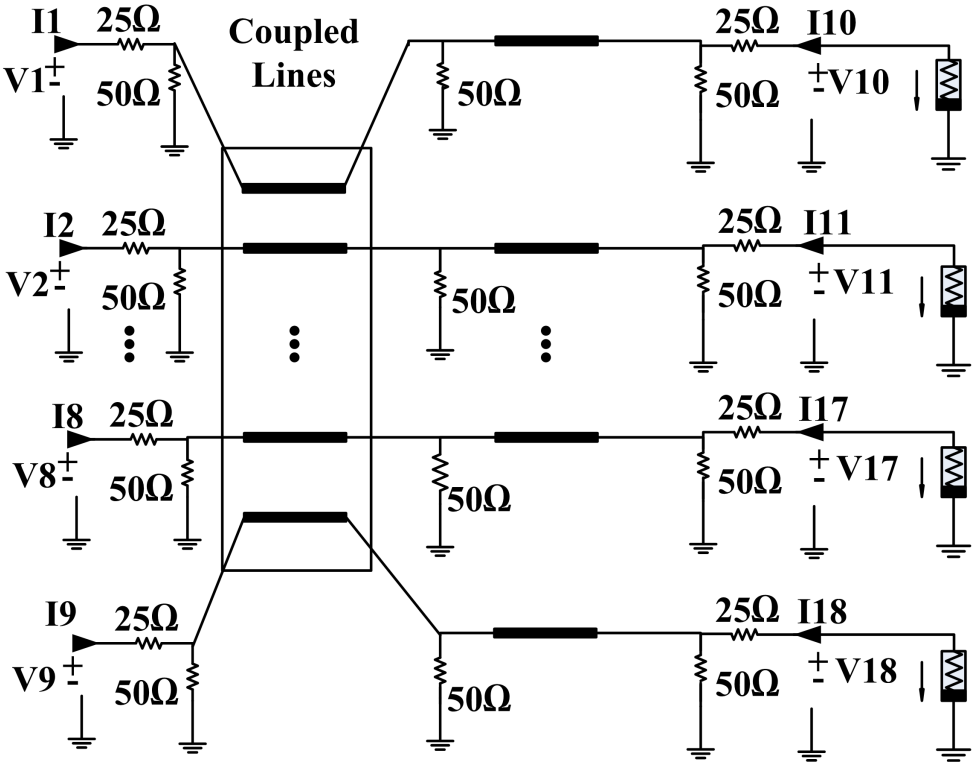

Figure 4.9: Circuit of (Example 4)

4.4.4 Example 4

This example is the 18-port example from Chapter 3. Nine nonlinear elements are added at the termiation of port 10 to port 18 depicted in Figure 4.9. For this example, Loewner matrix

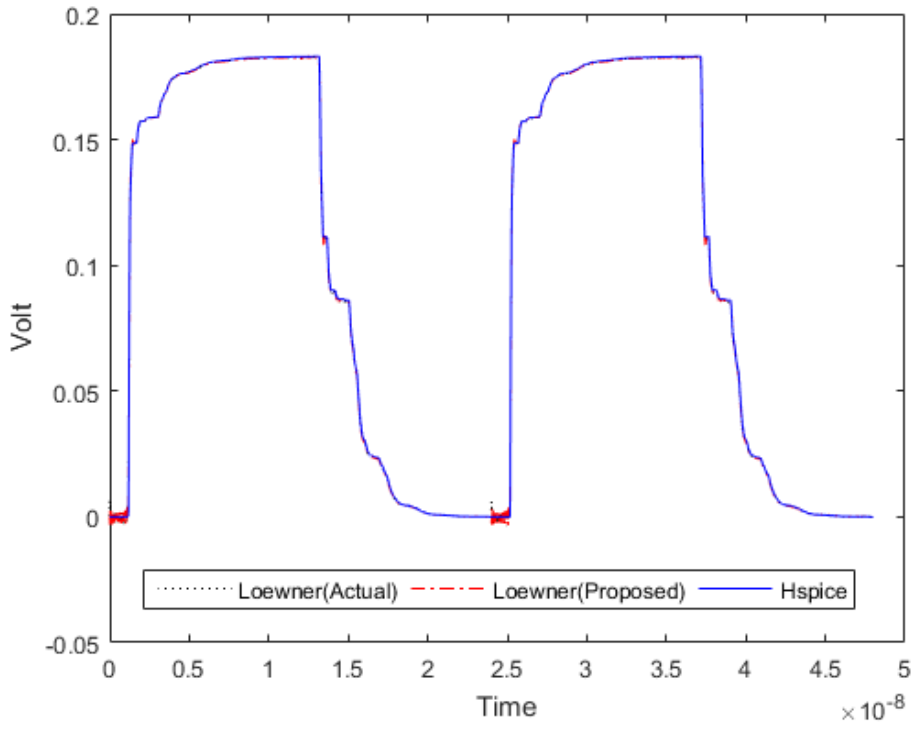

Figure 4.10: Transient Analysis at port 10 (Example 4)

modeling has been used. Port frequency data has been acquired from Hspice simulation. Here applied voltage at Port-1 is a trapezoidal pulse with a rise and fall time of 0.1 ns, a pulsewidth of 12.1 ns and a magnitude of 1V. The transient simulation at port 10 is shown in Figure 4.10 applying conventional matrix inversion (actual) and proposed methods incorporation with Loewner modeling and Hspice simulation.

Simulation time results between conventional matrix inversion and LCS approach have been given in Table 4.1 for these four examples. We can have 2.20 to 3.26 time faster simulation time using our proposed method than the matrix inversion technique.

4.5 Limitations of Proposed LCS Method

In our proposed algorithm, we have considered time step size as a constant. If the step size changes, large linear matrices change at each time step. Therefore, LU decomposition of the

large linear matrices needs to be done at each time step. As a result, we will not get any speed up from this method. Another criteria has been considered here is nonlinear elements are very few compared to linear elements. If nonlinear element matrix size is equal to linear matrix size then our proposed algorithm will not give any speed up. To gain speed up, nonlinear elements must be of very small numbers compared to linear elements.

4.6 Conclusion

In this chapter, two macromodeling approaches have been used for time domain analysis of distributed networks with nonlinear elements. For both modeling methods, LCS approach has been used. From the results given in Table 4.2 we can see that, proposed approach can be done 2.20 to 3.26 times faster than the conventional matrix inversion approach. A number of examples were presented showing the accuracy of the LCS method compared to the matrix inversion technique.

Chapter 5

Summary and Future Work

5.1 Summary

In chapter 2, an overview of different macromodeling techniques has been presented. These methods acknowledge both categories where there is knowledge for the physical characteristics and dimensions of the structure available and when the model is derived from the measured tabulated data. Loewner Matrix method has been proposed to identify a system from measured frequency data. In this thesis, two issues have been addressed. The first is that in the presence of noise Loewner matrix method has issues to identify the system from tabulated data. Another issue is associated with time domain simulation of interconnect networks with nonlinear drivers and loads. After macromodeling high speed interconnects using lumped or Loewner modeling linear networks become large matrices making time domain analysis a CPU intensive task for circuit simulators with nonlinear components.

In chapter 3, an iterative Loewner method is proposed to approximate the eigenvectors from previously approximated Loewner model. We can see that using this iterative approximation, eigenvectors become less noisy and this improves the approximation of the rational transfer function using this method. An order selection approach is also described here to select the best order to approximate the system. Numerical examples are presented here to validate the

accuracy of the proposed method.

In chapter 4, a faster time domain simulation approach has been proposed using Large Change Sensitivity approach. Interconnect networks have been modeled using lumped modeling and Loewner modeling approaches. In conventional approach to perform transient simulation, circuit equations are solved at each time point with one LU decomposition and one forward/backward substitution. Using Large Change Sensitivity approach linear parts are partitioned from nonlinear parts. As a result, in transient analysis only the nonlinear part is inverted and the linear part remains same. Nonlinear part is smaller compared to the linear part. Cost of inverting a large matrix is much more than inverting a smaller one. As a result, time domain simulation becomes faster using the proposed approach. For both of the modeling approaches, LCS algorithm is faster than the conventional matrix inversion method.

5.2 Future Work

Based on the work presented in this thesis, some suggestions for future work are provided here in this section as follows,

1. Delay extraction based Loewner modeling approach has been used for long interconnects [32]. Our proposed iterative Loewner modeling along with delay extraction can be used for further improvement of the rational approximation. One advantage of using delay extraction is that it will give low-order approximation for the frequency domain noisy data.

2. Large Change Sensitivity approach has been used for fast time domain analysis for all the variables of the system. To check the reliability of the system, sometimes we do not need to calculate all the variables of the system. We only need some variables to be calculated. An adjoint approach can be applied to calculate a few variables of the system. The issue of applying this adjoint approach is we need knowledge on all system variables for time domain analysis of adjoint network. A variational approach presented in [59] can be used to solve this issue. The adjoint network can be solved backward in time without having knowledge of the

system variables. By applying adjoint approach incorporation with LCS method can make time domain analysis much faster.

3. Another approach known as Barycentric vector fitting has been recently proposed to approximate multiport measured data [60]. In this approach interpolation approach of the points is different than Vector fitting algorithm. This approach is faster than Vector fitting approach for multiport system. To improve convergence and accuracy of Barycentric vector fitting an instrumental variable approach like [35] can be applied in the step where the coefficients of the rational approximation are determined in a least square sense. This will minimize the biasing effect of the least square solution caused by the noisy data. These instruments will be generated from the rational approximation of the previous iteration. As a result, computational complexity of Barycentric vector fitting will not be increased.

Bibliography

[1] R. A. Sainati and T. J. Moravec, "Estimating high speed circuit interconnect performance," *IEEE Trans. Circuits Syst*, vol. 36, no. 4, pp. 533–541, Apr. 1989.

[2] C. R. Paul, *Analysis of multiconductor transmission lines*. John Wiley & Sons, 2008.

[3] R. Achar and M. S. Nakhla, "Simulation of high-speed interconnects," *Proc. IEEE*, vol. 89, no. 5, pp. 693–728, May 2001.

[4] A. Deutsch, "Electrical characteristics of interconnections for high-performance systems," *Proc. IEEE*, vol. 86, no. 2, pp. 315–357, 1998.

[5] A. E. Ruehli and A. C. Cangellaris, "Progress in the methodologies for the electrical modeling of interconnects and electronic packages," *Proc. IEEE*, vol. 89, no. 5, pp. 740–771, May 2001.

[6] A. Dounavis, R. Achar, and M. S. Nakhla, "Addressing transient errors in passive macromodels of distributed transmission-line networks," *IEEE Trans. Microw. Theory Techn.*, vol. 50, no. 12, pp. 2759–2768, Dec 2002.

[7] A. Beygi, "Time-domain macromodeling of high speed distributed networks," Ph.D. dissertation, The University of Western Ontario, 2011.

[8] T. Dhaene and D. de Zutter, "Selection of lumped element models for coupled lossy transmission lines," *IEEE Trans. Comput.-Aided Design Integr. Circuits Syst.*, vol. 11, no. 7, pp. 805–815, Jul 1992.

[9] A. Odabasioglu, M. Celik, and L. T. Pileggi, "Prima: passive reduced-order interconnect macromodeling algorithm," *IEEE Trans. Comput.-Aided Design Integr. Circuits Syst.*, vol. 17, no. 8, pp. 645–654, Aug 1998.

[10] A. Dounavis, R. Achar, and M. S. Nakhla, "Efficient passive circuit models for distributed networks with frequency-dependent parameters," *IEEE Trans. Adv. Packag.*, vol. 23, no. 3, pp. 382–392, Aug 2000.

[11] A. Dounavis, R. Achar, and M. Nakhla, "A general class of passive macromodels for lossy multiconductor transmission lines," *IEEE Trans. Microw. Theory Techn.*, vol. 49, no. 10, pp. 1686–1696, Oct 2001.

[12] A. C. Cangellaris, S. Pasha, J. L. Prince, and M. Celik, "A new discrete transmission line model for passive model order reduction and macromodeling of high-speed interconnections," *IEEE Trans. Adv. Packag.*, vol. 22, no. 3, pp. 356–364, Aug 1999.

[13] Q. Yu, J. M. L. Wang, and E. S. Kuh, "Passive multipoint moment matching model order reduction algorithm on multiport distributed interconnect networks," *IEEE Trans. Circuits Syst. I*, vol. 46, no. 1, pp. 140–160, Jan 1999.

[14] E. Gad and M. Nakhla, "Efficient simulation of nonuniform transmission lines using integrated congruence transform," *IEEE Transactions on Very Large Scale Integration (VLSI) Systems*, vol. 12, no. 12, pp. 1307–1320, Dec 2004.

[15] F. H. Branin, "Transient analysis of lossless transmission lines," *Proc. IEEE*, vol. 55, no. 11, pp. 2012–2013, Nov 1967.

[16] B. Gustavsen and A. Semlyen, "Rational approximation of frequency domain responses by vector fitting," *IEEE Trans. Power Del.*, vol. 14, no. 3, pp. 1052–1061, Jul 1999.

[17] D. Saraswat, R. Achar, and M. S. Nakhla, "A fast algorithm and practical considerations for passive macromodeling of measured/simulated data," *IEEE Trans. Adv. Packag.*, vol. 27, no. 1, pp. 57–70, Feb 2004.

[18] C. P. Coelho, J. Phillips, and L. M. Silveira, "A convex programming approach for generating guaranteed passive approximations to tabulated frequency-data," *IEEE Trans. Comput.-Aided Design Integr. Circuits Syst.*, vol. 23, no. 2, pp. 293–301, Feb 2004.

[19] J. E. Schutt-Aine and R. Mittra, "Scattering parameter transient analysis of transmission lines loaded with nonlinear terminations," *IEEE Trans. Microw. Theory Techn.*, vol. 36, no. 3, pp. 529–536, Mar 1988.

[20] A. R. Djordjevic, T. K. Sarkar, and R. F. Harrington, "Analysis of lossy transmission lines with arbitrary nonlinear terminal networks," *IEEE Trans. Microw. Theory Techn.*, vol. 34, no. 6, pp. 660–666, Jun 1986.

[21] W. T. Beyene and J. Schutt-Aine, "Accurate frequency-domain modeling and efficient circuit simulation of high-speed packaging interconnects," *IEEE Trans. Microw. Theory Techn.*, vol. 45, no. 10, pp. 1941–1947, Oct 1997.

[22] S. Lin and E. S. Kuh, "Transient simulation of lossy interconnects based on the recursive convolution formulation," *IEEE Trans. Circuits Syst. I*, vol. 39, no. 11, pp. 879–892, Nov 1992.

[23] C.-W. Ho, A. Ruehli, and P. Brennan, "The modified nodal approach to network analysis," *IEEE Transactions on Circuits and Systems*, vol. 22, no. 6, pp. 504–509, Jun 1975.

[24] S. B. Olivadese, S. Grivet-Talocia, C. Siviero, and D. Kaller, "Macromodel-based iterative solvers for simulation of high-speed links with nonlinear terminations," *IEEE Trans. Compon. Packag. Manuf. Technol.*, vol. 4, no. 11, pp. 1847–1861, Nov 2014.

[25] B. Gustavsen and A. Semlyen, "A robust approach for system identification in the frequency domain," *IEEE Trans. Power Del.*, vol. 19, no. 3, pp. 1167–1173, July 2004.

[26] B. Gustavsen, "Improving the pole relocating properties of vector fitting," *IEEE Trans. Power Del.*, vol. 21, no. 3, pp. 1587–1592, July 2006.

[27] D. Deschrijver, M. Mrozowski, T. Dhaene, and D. D. Zutter, "Macromodeling of multiport systems using a fast implementation of the vector fitting method," *IEEE Microw. Wireless Compon. Lett.*, vol. 18, no. 6, pp. 383–385, June 2008.

[28] A. Chinea and S. Grivet-Talocia, "On the parallelization of vector fitting algorithms," *IEEE Trans. Compon. Packag. Manuf. Technol.*, vol. 1, no. 11, pp. 1761–1773, Nov 2011.

[29] S. Lefteriu and A. C. Antoulas, "A new approach to modeling multiport systems from frequency-domain data," *IEEE Trans. Comput.-Aided Design Integr. Circuits Syst.*, vol. 29, no. 1, pp. 14–27, Jan 2010.

[30] Y. Wang, C. U. Lei, G. K. H. Pang, and N. Wong, " MFTI : Matrix-format tangential interpolation for modeling multi-port systems," in *Design Automation Conference (DAC), 2010 47th ACM/IEEE*, June 2010, pp. 683–686.

[31] M. Kabir and R. Khazaka, "Macromodeling of distributed networks from frequency-domain data using the loewner matrix approach," *IEEE Trans. Microw. Theory Techn.*, vol. 60, no. 12, pp. 3927–3938, Dec 2012.

[32] M. Sahouli and A. Dounavis, "Delay extraction-based modeling using loewner matrix framework," *IEEE Trans. Compon. Packag. Manuf. Technol.*, vol. 7, no. 3, pp. 424–433, March 2017.

[33] S. Grivet-Talocia and M. Bandinu, "Improving the convergence of vector fitting for equivalent circuit extraction from noisy frequency responses," *IEEE Transactions on Electromagnetic Compatibility*, vol. 48, no. 1, pp. 104–120, Feb 2006.

[34] F. Ferranti, Y. Rolain, L. Knockaert, and T. Dhaene, "Variance weighted vector fitting for noisy frequency responses," *IEEE Microw. Wireless Compon. Lett.*, vol. 20, no. 4, pp. 187–189, April 2010.

[35] A. Beygi and A. Dounavis, "An instrumental variable vector-fitting approach for noisy frequency responses," *IEEE Trans. Microw. Theory Techn.*, vol. 60, no. 9, pp. 2702–2712, Sept 2012.

[36] S. Lefteriu, A. C. Ionita, and A. C. Antoulas, "Modeling systems based on noisy frequency and time domain measurements," in *Perspectives in Mathematical System Theory, Control, and Signal Processing*. Springer, 2010, pp. 365–378.

[37] M. Kabir, Y. Q. Xiao, and R. Khazaka, "Loewner matrix interpolation for noisy s-parameter data," in *2016 IEEE 25th Conference on Electrical Performance Of Electronic Packaging And Systems (EPEPS)*, Oct 2016, pp. 95–98.

[38] K. Singhal and J. Vlach, "Symbolic circuit analysis," *IEE Proc. G - Electronic Circuits and Systems*, vol. 128, no. 2, pp. 81–86, Apr. 1981.

[39] J. Vlach and K. Singhal, *Computer Methods for Circuit Analysis and Design*. Springer Science & Business Media, 1983.

[40] B. Ramachandra Achar, "Model-reduction techniques for high-speed interconnect analysis," Ph.D. dissertation, Carleton University Ottawa, Canada, 1998.

[41] "HSPICE U-2003.09-RA," Synopsys Inc., CA.

[42] I. M. Elfadel, H.-M. Huang, A. E. Ruehli, A. Dounavis, and M. S. Nakhla, "A comparative study of two transient analysis algorithms for lossy transmission lines with frequency-dependent data," *IEEE Trans. Adv. Packag.*, vol. 25, no. 2, pp. 143–153, May 2002.

[43] F. Y. Chang, "The generalized method of characteristics for waveform relaxation analysis of lossy coupled transmission lines," *IEEE Trans. Microw. Theory Techn.*, vol. 37, no. 12, pp. 2028–2038, Dec 1989.

[44] D. B. Kuznetsov and J. E. Schutt-Aine, "Optimal transient simulation of transmission lines," *IEEE Trans. Circuits Syst. I*, vol. 43, no. 2, pp. 110–121, Feb 1996.

[45] S. Grivet-Talocia, H.-M. Huang, A. E. Ruehli, F. Canavero, and I. M. Elfadel, "Transient analysis of lossy transmission lines: an efficient approach based on the method of characteristics," *IEEE Trans. Adv. Packag.*, vol. 27, no. 1, pp. 45–56, Feb 2004.

[46] M. S. Nakhla, "Analysis of pulse propagation on high-speed vlsi chips," *IEEE Journal of Solid-State Circuits*, vol. 25, no. 2, pp. 490–494, Apr 1990.

[47] R. Wang and O. Wing, "A circuit model of a system of vlsi interconnects for time response computation," *IEEE Trans. Microw. Theory Techn.*, vol. 39, no. 4, pp. 688–693, Apr 1991.

[48] R. Achar, M. S. Nakhla, and Q. J. Zhang, "Addressing high frequency effects in vlsi interconnects with full wave model and cfh," in *Proceedings of IEEE International Conference on Computer Aided Design (ICCAD)*, Nov 1995, pp. 53–56.

[49] M. Celik, A. C. Cangellaris, and A. Deutsch, "A new moment generation technique for interconnects characterized by measured or calculated s-parameters," in *Proceedings 1996 IEEE Multi-Chip Module Conference (Cat. No.96CH35893)*, Feb 1996, pp. 196–201.

[50] G. Zheng, Q.-J. Zhang, M. Nakhla, and R. Achar, "An efficient approach for moment-matching simulation of linear subnetworks with measured or tabulated data," in *Proceedings of International Conference on Computer Aided Design*, Nov 1996, pp. 20–23.

[51] M. Piket-May, A. Taflove, and J. Baron, "FD-TD modeling of digital signal propagation in 3-d circuits with passive and active loads," *IEEE Trans. Microw. Theory Techn.*, vol. 42, no. 8, pp. 1514–1523, Aug 1994.

[52] P. C. Cherry and M. F. Iskander, "FDTD analysis of high frequency electronic interconnection effects," *IEEE Trans. Microw. Theory Techn.*, vol. 43, no. 10, pp. 2445–2451, Oct 1995.

[53] S. D. Corey and A. T. Yang, "Interconnect characterization using time-domain reflectometry," *IEEE Trans. Microw. Theory Techn.*, vol. 43, no. 9, pp. 2151–2156, Sep 1995.

[54] B. Gustavsen and A. Semlyen, "Simulation of transmission line transients using vector fitting and modal decomposition," *IEEE Trans. Power Del.*, vol. 13, no. 2, pp. 605–614, Apr 1998.

[55] S. Grivet-Talocia, "Package macromodeling via time-domain vector fitting," *IEEE Microw. Wireless Compon. Lett.*, vol. 13, no. 11, pp. 472–474, Nov 2003.

[56] D. Deschrijver and T. Dhaene, "Passivity-based sample selection and adaptive vector fitting algorithm for pole-residue modeling of sparse frequency-domain data," in *Proceedings of the 2004 IEEE International Behavioral Modeling and Simulation Conference, 2004. BMAS 2004.*, Oct 2004, pp. 68–73.

[57] T. Dhaene and D. Deschrijver, "Generalised vector fitting algorithm for macromodelling of passive electronic components," *Electronics Letters*, vol. 41, no. 6, pp. 299–300, March 2005.

[58] A. C. Cangellaris and A. E. Ruehli, "Model order reduction techniques applied to electromagnetic problems," in *IEEE 9th Topical Meeting on Electrical Performance of Electronic Packaging (Cat. No.00TH8524)*, 2000, pp. 239–242.

[59] S. Lum, M. Nakhla, and Q.-J. Zhang, "Sensitivity analysis of lossy coupled transmission lines with nonlinear terminations," *IEEE Trans. Microw. Theory Techn.*, vol. 42, no. 4, pp. 607–615, Apr. 1994.

[60] D. Deschrijver, L. Knockaert, and T. Dhaene, “A barycentric vector fitting algorithm for efficient macromodeling of linear multiport systems,” *IEEE Microw. Wireless Compon. Lett.*, vol. 23, no. 2, pp. 60–62, Feb 2013.

Curriculum Vitae

Name:	Sadia Wahid
Post-Secondary Education and Degrees:	Bangladesh University of Engineering and Technology Dhaka, Bangladesh 2008 - 2013 B.Sc.
Related Work Experience:	Research Assistant The University of Western Ontario 2015 - 2017 Teaching Assistant The University of Western Ontario 2016 - 2017